

Phenomenology of bond and flux orders in kagome metals

Glenn Wagner,¹ Chunyu Guo,² Philip J. W. Moll,² Titus Neupert,¹ and Mark H. Fischer¹

¹*Department of Physics, University of Zurich, Winterthurerstrasse 190, 8057 Zurich, Switzerland*

²*Max Planck Institute for the Structure and Dynamics of Matter, Hamburg, Germany*

Despite much experimental and theoretical work, the nature of the charge order in the kagome metals belonging to the family of materials AV_3Sb_5 ($A=Cs,Rb,K$) remains controversial. A crucial ingredient for the identification of the ordering in these materials is their response to external perturbations, such as strain or magnetic fields. To this end, we provide a comprehensive symmetry classification of the possible charge orders in kagome materials with a 2×2 increase of the unit cell. Motivated by the experimental reports of time-reversal-symmetry breaking and rotational anisotropy, we consider the interdependence of flux and bond orders. Deriving the relevant Landau free energy for possible orders, we study the effect of symmetry-breaking perturbations such as strain and magnetic fields. Our results, thus, provide a roadmap for future tests of these intricate orders.

I. INTRODUCTION

Starting with the formation of crystalline materials, spontaneous symmetry breaking is a concept foundational to condensed matter physics and guides our categorical understanding of phases of matter [1]. Charge order can break spatial symmetries in the form of nematicity (rotational symmetry) or density waves (translational symmetry), superconductors break particle number conservation, magnets break spin-rotation and time-reversal symmetry (TRS). Particularly interesting situations arise, when the order comprises multiple degenerate components, in other words when the irreducible representation (irrep) corresponding to the order is multi-dimensional or when order parameters from different irreps are (accidentally) almost degenerate. On the one hand, this situation can lead to additional breaking of symmetries: in the case of a superconductor, a complex superposition of two order-parameter components leads to a chiral superconductor spontaneously breaking TRS [2]. On the other hand, multi-component orders can also help restore symmetries: A $\mathbf{q} = (\pi, 0)$ charge order breaks both translation and rotation symmetry, while a superposition of $(\pi, 0)$ and $(0, \pi)$ charge order describes checkerboard order and restores rotational symmetry [3].

A charge order of unconventional nature has recently been identified in a family of quasi-two-dimensional metals AV_3Sb_5 ($A=Cs,Rb,K$), whose main structural motif is a kagome lattice of vanadium atoms [4, 5]. The charge-ordered phase, which sets in at about 70–100 K, has been studied with a variety of experimental techniques including angle-resolved photoemission spectroscopy [6, 7], scanning tunneling spectroscopy [8–12], nuclear magnetic resonance [10, 13, 14], X-ray scattering [15], muon spin-relaxation measurements [16, 17], thermal [18] and electrical [10, 18–25] transport, as well as magneto-optical Kerr effect [26–29]. Broad consensus exists that the charge order creates a 2×2 superstructure within the plane, whereas the out-of-plane ordering (such as $2 \times 2 \times 1$, $2 \times 2 \times 2$ or $2 \times 2 \times 4$) is still under debate [30, 31]. In addition, controversial results as to whether or not charge or-

der spontaneously breaks time-reversal and/or rotational symmetry have been reported. Several phenomena usually associated with spontaneous TRS breaking (TRSB) can be induced by a (weak) magnetic field, such as a giant anomalous Hall effect [32–34] and non-vanishing Kerr rotations [28]. However, whether the system breaks time-reversal symmetry spontaneously, in other words at zero magnetic field, has been challenged for instance by the absence of a Kerr effect in this regime [28]. Furthermore, although there are some reports of TRSB at the charge-ordering temperature, there is a large increase in the respective signals around 30–50 K. Finally, while there are many reports of (rotational) anisotropy in these materials [10, 35–37], a recent study challenges these reports [24].

The conflicting experimental reports of anisotropy and spontaneous TRSB naturally raise the question whether the experiments themselves change the state probed and if so, how the different ordering possibilities can still be distinguished experimentally. Importantly, the interplay of different components of the order parameter is crucial, since charge-density-wave order on the kagome lattice with an ordering vector $\mathbf{Q} = \mathbf{M} = \overline{\Gamma M}$ forms a three-dimensional irrep due to the three inequivalent M points. A single order-parameter component, corresponding to a single M -point ordering vector, breaks the rotational symmetry, whereas an equal superposition of all three could restore the rotational symmetry of the lattice. Furthermore, a complex order, arising due to the superposition of (almost degenerate) bond order and flux order would lead to TRSB.

To understand the physics of charge density waves in the kagome systems better and discuss their coupling to external perturbations that could help identify them, such as magnetic fields or strain, the proper symmetry of the ordering possibilities need to be studied first. Such an analysis then allows for the derivation of an effective Landau description. While both electronic [38] and phonon [31, 39] instabilities have been studied as mechanisms for the charge ordering in the literature, such an approach has the advantage of being agnostic to the microscopic mechanism of the ordering.

Here, we present a comprehensive symmetry classi-

fication of all in-plane charge orders—including onsite charge modulations, bond orders, and flux/orbital current orders—on the kagome lattice with 2×2 unit cell following the scheme introduced in Ref. [40]. This classification scheme provides a transparent way to develop an effective theory in the spirit of a Landau free energy for all charge orders, their coupling to each other and to magnetic fields and strain. This theory is applicable to, but not limited to, AV_3Sb_5 . Since flux and bond orders both renormalize electron hopping integrals, we consider them intertwined. However, with the two generically transforming as different irreps, we treat them as different, yet coupled, order parameters, instead of one single complex order parameter. We therefore do not adopt the usual presumption that one order parameter dominates at and near the phase transition, but we study the interplay of one flux and one bond order parameter. This consideration results in a few scenarios, which can be sharply distinguished experimentally through their behavior in a magnetic field and by the presence or absence of anisotropy.

II. SUMMARY OF RESULTS

We start by considering only in-plane ordering. Motivated by experiments that have established a 2×2 in-plane increase in the unit cell size, we consider all possible charge, bond, and flux orders on the kagome lattice arising from nearest-neighbor interactions. In Sec. III, we use a group theory analysis to classify all these orders within the framework introduced by Venderbos [40]. The translational-symmetry-breaking orders can be classified in four different irreps of the (enlarged) symmetry group, labelled F_1, \dots, F_4 . The irreps are three-dimensional and $F_{1,2}$ are even under C_2 while $F_{3,4}$ are odd. Bond order Δ can fall in any of the four translationally symmetry breaking irreps, while flux order Δ' has to either fall in the F_2 or F_4 irrep.

The observation of time-reversal-symmetry breaking shows that flux order is present (although whether or not a small magnetic field is necessary to establish the flux order is not clear). Bond and flux order naturally couple to one another and in Sec. IV, we therefore consider Landau theories that include both orders. The second and fourth order terms in the free energy are identical regardless of which orders are combined, since these terms are always C_2 symmetric. However, the third-order terms can differ, since they are not guaranteed to respect C_2 . If the bond order is even under C_2 , then a term of the form Δ^3 is allowed. In addition the bond and flux order can couple via $\Delta\Delta'^2$ (the C_2 eigenvalue of the flux is irrelevant here, since the flux order needs to appear squared for the free energy to respect time-reversal symmetry).

To gain intuition about the Landau free energy, in Sec. V we start by discussing the simpler case where only charge order is present. We discuss separately the cases where a third-order term is present or absent, since this

significantly impacts the phase diagram. In Sec. VI, we then discuss the more complicated case with both charge and flux order present. We again derive the phase diagrams for the cases with and without the third-order term. In the phase diagrams, we use the relative critical temperature of the bond and flux orders as a tuning parameter. We obtain three types of phases: Either only Δ or only Δ' is present, or both are present simultaneously. The latter two phases break time-reversal symmetry. These different phases may or may not spontaneously break the C_6 symmetry depending on the specific irreps of the respective orders.

One way to distinguish the different possible order parameters is to consider the impact of symmetry-breaking perturbations. In Sec. VII, we therefore investigate the effects of strain and an out-of-plane magnetic field. The lowest-order coupling to such a magnetic field B takes the form $B\Delta\Delta'$. Since the magnetic field is odd under in-plane mirror symmetries, this term is only allowed when the product $\Delta\Delta'$ is odd under these mirrors.

Up to this point, the Landau theory considered was very general and relied only on well-established experimental facts on the kagome metals. In Sec. VIII, we review the experimental situation in more detail and suggest that the most likely order parameter combination to describe the experiments is a F_1 bond order with a F_2 flux order. Note, however, that while this conclusion relies on experimental input that is less well-established, we emphasize that the general discussion does not.

Finally, in Sec. IX we propose several experiments including elastoresistance, STM and resonant ultrasound spectroscopy that in combination with the Landau analysis would allow to clearly establish the type of ordering in the kagome metals.

III. SYMMETRY ANALYSIS

In the following, we consider a single kagome layer with point group C_{6v} [41]. Further, we study translational symmetry breaking arising from M -point ordering vectors in the kagome Brillouin zone. This ordering vector arises due to three van-Hove singularities (VHS) of the band structure of the kagome lattice at the three M points [42]:

$$\mathbf{M}_{1,3} = \frac{\pi}{a\sqrt{3}}(\pm\sqrt{3}, 1), \quad \mathbf{M}_2 = \frac{2\pi}{a\sqrt{3}}(0, -1), \quad (1)$$

where a is the lattice constant. Close to the van Hove filling, the low-energy physics is dominated by scattering between these VHS, with momentum transfers corresponding to momentum differences between the M -points. These nesting vectors are also M -point vectors, since $\mathbf{M}_2 - \mathbf{M}_3 \equiv \mathbf{M}_1$ (up to a reciprocal lattice vector) and the order parameters consist of superpositions of waves with wavevectors \mathbf{M}_i . Therefore, the order parameter in the unit cell centered at \mathbf{R} will be a linear

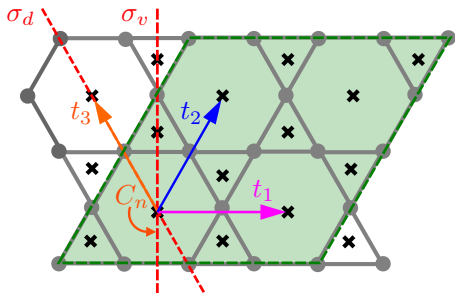


FIG. 1. Schematic of the 2×2 enlarged unit cell of the kagome lattice with definitions of the elements of C_{6v}''' . We define the three translation operations t_i , mirror reflections σ_v, σ_d and rotations C_n with $n = 2, 3, 6$. Sites and bonds are indicated in grey, while plaquettes are indicated by a black cross. There are 12 sites, 24 bonds and 12 plaquettes within the 2×2 enlarged unit cell (green shading).

superposition of the components of

$$\mathbf{v}(\mathbf{R}) = \begin{pmatrix} \cos \mathbf{M}_1 \cdot \mathbf{R} \\ \cos \mathbf{M}_2 \cdot \mathbf{R} \\ \cos \mathbf{M}_3 \cdot \mathbf{R} \end{pmatrix} \quad (2)$$

leading to an increase in the size of the unit cell by 2×2 . The corresponding Bragg peaks are indeed seen experimentally in X-ray diffraction [6, 30, 43] and STM [8, 9, 11, 44].

The possible bond and flux orders have been classified previously in Refs. 45 and 46 regarding the point group D_{6h} . We here choose a different route by following the classification scheme introduced in Ref. 40 and restricting ourselves to the point group C_{6v} for simplicity. In this real-space scheme, the relevant symmetry group is enlarged to C_{6v}''' , where the primes indicate that the point group of the kagome lattice, C_{6v} , contains three additional elements corresponding to translations \mathbf{t}_i (with $i = 1, 2, 3$) that describe the translational symmetry breaking. The enlarged unit cell as well as the symmetry operations forming the group C_{6v}''' are shown in Fig. 1. The group C_{6v}''' has four one-dimensional and two two-dimensional irreps that are trivial under translation and are thus simply analogous to the irreps of C_{6v} . There are also four three-dimensional irreps F_i , which, in contrast, are non-trivial under translations. Their dimensionality directly follows from the fact that there are three M points in the Brillouin zone. Table I presents the character table for the irreps of C_{6v}''' .

There are three fundamental types of order, which, following the nomenclature adapted in Ref. 40, we denote as site, bond, and flux order, with the latter two being real and imaginary renormalizations of the hopping integrals. We deduce which irreps of C_{6v}''' these orders on the kagome lattice decompose into, considering only nearest-neighbor order for the bond and flux order. To do so, we consider the permutation matrices \mathcal{P} describing the action of the symmetry operators on the sites, bonds and fluxes. These permutation matrices are representations

	I	t_i	C_2	$t_i C_2$	C_3	C_6	σ_v	$t_i \sigma_v$	σ_d	$t_i \sigma_d$
$[\mathcal{C}]$	1	3	1	3	8	8	6	6	6	6
A_1	1	1	1	1	1	1	1	1	1	1
A_2	1	1	1	1	1	1	-1	-1	-1	-1
B_1	1	1	-1	-1	1	-1	1	1	-1	-1
B_2	1	1	-1	-1	1	-1	-1	-1	1	1
E_1	2	2	-2	-2	-1	1	0	0	0	0
E_2	2	2	2	2	-1	-1	0	0	0	0
F_1	3	-1	3	-1	0	0	1	-1	1	-1
F_2	3	-1	3	-1	0	0	-1	1	-1	1
F_3	3	-1	-3	1	0	0	1	-1	-1	1
F_4	3	-1	-3	1	0	0	-1	1	1	-1

TABLE I. Character table of the group C_{6v}''' [40]. The one- and two-dimensional irreps preserve the translation symmetry of the original kagome lattice, while the three-dimensional irreps lead to a 2×2 increase in the unit cell.

of C_{6v}''' and, using the character Tab. I, they can be decomposed into irreps, see appendix A.

Site order corresponds to a modulation of $\langle a_{i\sigma}^\dagger(\mathbf{R}) a_{i\sigma}(\mathbf{R}) \rangle$, the local electron density, where $a_{i\sigma}^\dagger(\mathbf{R})$ creates an electron with spin $\sigma = \uparrow, \downarrow$ at a position $\mathbf{R} + \delta_i$. Here, \mathbf{R} points to the unit cell center and δ_i is the position of the sublattice site $i = A, B, C$ with respect to \mathbf{R} . Denoting the order-parameter components on each sublattice by a three-dimensional vector \mathbf{s}_i , the site order takes the form

$$\langle a_{i\sigma}^\dagger(\mathbf{R}) a_{i\sigma}(\mathbf{R}) \rangle = \mathbf{s}_i \cdot \mathbf{v}(\mathbf{R}). \quad (3)$$

With 12 sites in the 2×2 -increased unit cell, the representation is 12 dimensional. The possible site orders then decompose into the following irreps

$$\mathcal{P}_s = A_1 + E_2 + F_1 + F_3 + F_4. \quad (4)$$

A general bond order corresponds to modulations

$$\begin{aligned} \langle a_{A\sigma}^\dagger(\mathbf{R}) a_{B\sigma}(\mathbf{R}) \rangle &= \mathbf{w}_1 \cdot \mathbf{v}(\mathbf{R}) \\ \langle a_{A\sigma}^\dagger(\mathbf{R}) a_{C\sigma}(\mathbf{R}) \rangle &= \mathbf{w}_2 \cdot \mathbf{v}(\mathbf{R}) \\ \langle a_{A\sigma}^\dagger(\mathbf{R}) a_{B\sigma}(\mathbf{R} - \mathbf{t}_3) \rangle &= \mathbf{w}_3 \cdot \mathbf{v}(\mathbf{R}) \\ \langle a_{A\sigma}^\dagger(\mathbf{R}) a_{C\sigma}(\mathbf{R} + \mathbf{t}_2) \rangle &= \mathbf{w}_4 \cdot \mathbf{v}(\mathbf{R}) \\ \langle a_{B\sigma}^\dagger(\mathbf{R}) a_{C\sigma}(\mathbf{R} + \mathbf{t}_2) \rangle &= \mathbf{w}_5 \cdot \mathbf{v}(\mathbf{R}) \\ \langle a_{C\sigma}^\dagger(\mathbf{R}) a_{B\sigma}(\mathbf{R} - \mathbf{t}_3) \rangle &= \mathbf{w}_6 \cdot \mathbf{v}(\mathbf{R}). \end{aligned} \quad (5)$$

We refer to real components of these \mathbf{w}_i as bond order. There are 24 bonds within the 2×2 unit cell and we find the bond order decomposition

$$\mathcal{P}_b = A_1 + B_1 + E_1 + E_2 + 2F_1 + F_2 + 2F_3 + F_4. \quad (6)$$

Finally, flux orders imply an imaginary component of the \mathbf{w}_i [47]. Equivalently, one can think of the resulting flux threading through the plaquettes. There are 12 plaquettes within the 2×2 enlarged unit cell with possible orders decomposing into the irreps

$$\mathcal{P}_\phi = 2A_2' + B_2' + 2F_2' + F_4'. \quad (7)$$

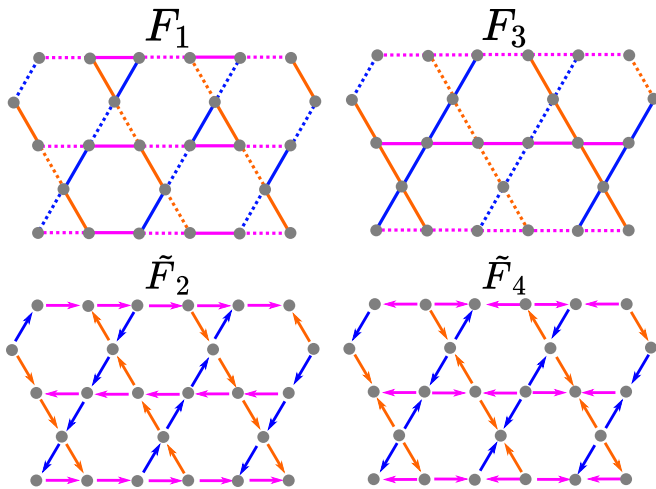


FIG. 2. Schematics of the bond order F_1, F_3 and flux orders F'_2, F'_4 . For the bond orders, solid (dashed) lines indicate positive (negative) values of the order parameter. Colors indicate the components $\Delta_1, \Delta_2, \Delta_3$ of the bond order parameter. For the flux order parameter the arrows indicate the direction of the current. Colors indicate the components $\Delta'_1, \Delta'_2, \Delta'_3$ of the flux order parameter.

In addition to spatial symmetries, the flux order breaks TRS, which we denote by a prime. Figure 2 shows examples of different types of translational symmetry breaking bond and flux orders for each of the four three-dimensional irreps.

IV. LANDAU THEORY

Having categorized the possible site, bond, and flux orders, we can construct the free energy within Landau theory for different order parameters and their combinations. Having constructing such free energies then allows us to map out possible phase diagrams of the kagome metals, which capture the interplay of these order parameters, before studying the effect of external perturbations. The different responses to external perturbations can provide distinguishing experimental signatures.

Previous theoretical work has already studied several types of Landau free energies for the kagome metals. In particular, Ref. 31 studied coupling between an M -point and an L -point order, and Ref. 48 studied the coupling between an imaginary M -point order and superconductivity. Finally, Refs. 38, 46, 49–52 studied coupling between real and imaginary M -point orders, which is the case we aim to study here. Such a combination of orders is motivated by the observation of TRSB in experiments, which indicates that flux order is present at least under certain circumstances. Furthermore, since flux and bond order are the imaginary and real components, respectively, of the same (nearest-neighbor) order parameter, it is natural to consider a theory including both.

However, most of the previous literature considered the

bond order parameter to be a complex number, hence mixing bond and flux order of our classification. While this might be physically motivated and suggests a proximity of one order to the other, the real and imaginary components generally transform as different irreps, which manifests itself in different critical temperatures in these combined theories. We, thus, follow a different approach and in the following use the results from the order-parameter classification of Sec. III with the multiplication Tab. II to write a family of free energies for two coupled order parameters transforming under two (different) three-dimensional irreps: a time-reversal symmetric F_i and a TRS breaking F'_j . In particular, with the free energy transforming as a scalar, only combinations of irreps, whose decomposition includes A_1 , can appear. For this purpose, we first derive the Landau free energy $\mathcal{F}[\Delta, \Delta']$ up to fourth order in the order parameters Δ and Δ' , before studying their coupling to strain and (out-of-plane) magnetic fields.

A. Homogeneous M -point free energy

The quadratic terms in the free energy take the same form, irrespective of the irrep combination. We include the temperature dependence to the quadratic coefficients

$$\mathcal{F}^{(2)}[\Delta, \Delta'] = \alpha(T - T_c)(\Delta_1^2 + \Delta_2^2 + \Delta_3^2) + \alpha'(T - T'_c)(\Delta_1'^2 + \Delta_2'^2 + \Delta_3'^2). \quad (8)$$

The parameter T_c (T'_c) is the temperature, at which the coefficient for the quadratic term in Δ (Δ') changes sign. While this sign change signals that the solution with vanishing order parameter becomes unstable, this temperature does not necessarily coincide with the critical temperature at which the order parameter acquires a non-zero value. The third-order terms, as well as the coupling between the order parameters can shift the critical temperature away from T_c (T'_c).

The third-order terms may or may not be allowed, depending on the transformation properties of the irreps, in particular, their transformation behavior under C_2 . In Tab. III, we list the allowed third-order terms for the different order-parameter combinations. When the terms are allowed, they take the form [49, 50]

$$\begin{aligned} \mathcal{F}^{(3,0)}[\Delta, \Delta'] &= \beta_1 \Delta_1 \Delta_2 \Delta_3 & (9) \\ \mathcal{F}^{(1,2)}[\Delta, \Delta'] &= \beta_2 (\Delta_1 \Delta'_2 \Delta'_3 + \Delta'_1 \Delta_2 \Delta'_3 + \Delta'_1 \Delta'_2 \Delta_3). & (10) \end{aligned}$$

The term $\mathcal{F}^{(3,0)}$ is allowed if $A_1 \subset F_i \otimes F_i \otimes F_i$, while the term $\mathcal{F}^{(1,2)}$ is allowed if $A_1 \subset F_i \otimes F'_j \otimes F'_j$. Due to time-reversal symmetry, there is neither a linear nor a cubic term for Δ' . Note that the third-order term in Eq. (10) couples Δ and Δ' in such a way that any finite Δ' induces a finite Δ order, but not the other way around. In other words, while the TRS-preserving bond order may exist by itself, a finite Δ' always induces bond

	A_1	A_2	B_1	B_2	E_1	E_2	F_1	F_2	F_3	F_4
A_1	A_1	A_2	B_1	B_2	E_1	E_2	F_1	F_2	F_3	F_4
A_2		A_1	B_2	B_1	E_1	E_2	F_2	F_1	F_4	F_3
B_1			A_1	A_2	E_2	E_1	F_3	F_4	F_1	F_2
B_2				A_1	E_2	E_1	F_4	F_3	F_2	F_1
E_1					$A_1 + A_2 + E_2$	$B_1 + B_2 + E_1$	$F_3 + F_4$	$F_3 + F_4$	$F_1 + F_2$	$F_1 + F_2$
E_2						$A_1 + A_2 + E_2$	$F_1 + F_2$	$F_1 + F_2$	$F_3 + F_4$	$F_3 + F_4$
F_1							$A_1 + E_2 + F_1 + F_2$	$A_2 + E_2 + F_1 + F_2$	$B_1 + E_1 + F_3 + F_4$	$B_2 + E_1 + F_3 + F_4$
F_2								$A_1 + E_2 + F_1 + F_2$	$B_2 + E_1 + F_3 + F_4$	$B_1 + E_1 + F_3 + F_4$
F_3									$A_1 + E_2 + F_1 + F_2$	$A_2 + E_2 + F_1 + F_2$
F_4										$A_1 + E_2 + F_1 + F_2$

TABLE II. The product of two irreps R_1 and R_2 can be decomposed into irreps of C_{6v}''' . The table is symmetric and for conciseness we only populate the upper triangle of the matrix.

		Flux order	
		F_2'	F_4'
Bond order	F_1	$F_1^3, F_1 F_2'^2, B F_1 F_2'$	$F_1^3, F_1 F_4'^2$
	F_2	$F_2^3, F_2 F_2'^2$	$F_2^3, F_2 F_4'^2$
	F_3	none	$B F_3 F_4'$
	F_4	none	none

TABLE III. Table of the allowed third-order terms and couplings to the magnetic field for a free energy constructed from order parameters transforming under a time-reversal symmetry F_i and a time-reversal symmetry breaking F_j' .

order transforming as F_1 and F_2 . In the following, we will see how the presence of these third-order terms significantly alters the phenomenology of the ordered phase as compared to the case without such terms.

The fourth-order terms are again generically the same for all order-parameter combinations [46, 49, 50]

$$\begin{aligned}
\mathcal{F}^{(4)} = & \lambda_1 (\Delta_1^2 + \Delta_2^2 + \Delta_3^2)^2 \\
& + \lambda_2 (\Delta_1'^2 + \Delta_2'^2 + \Delta_3'^2)^2 \\
& + \lambda_3 (\Delta_1^2 + \Delta_2^2 + \Delta_3^2) (\Delta_1'^2 + \Delta_2'^2 + \Delta_3'^2) \\
& + \lambda_4 (\Delta_1^2 \Delta_2^2 + \Delta_1^2 \Delta_3^2 + \Delta_2^2 \Delta_3^2) \\
& + \lambda_5 (\Delta_1'^2 \Delta_2'^2 + \Delta_1'^2 \Delta_3'^2 + \Delta_2'^2 \Delta_3'^2) \\
& + \lambda_6 (\Delta_1^2 \Delta_2'^2 + \Delta_1^2 \Delta_3'^2 + \Delta_2^2 \Delta_3'^2) \\
& + \Delta_1'^2 \Delta_2^2 + \Delta_1'^2 \Delta_3^2 + \Delta_2'^2 \Delta_3^2 \\
& + \lambda_7 (\Delta_1 \Delta_1' \Delta_2 \Delta_2' + \Delta_1 \Delta_1' \Delta_3 \Delta_3' + \Delta_2 \Delta_2' \Delta_3 \Delta_3').
\end{aligned} \tag{11}$$

The inclusion of the fourth-order terms is necessary for the thermodynamic stability of the free energy. Furthermore, in the absence of third-order terms, the fourth-order terms determine the form of the symmetry-breaking combination, such as anisotropic or TRS-breaking, below T_c . $\mathcal{F}^{(4)}$ can also couple Δ and Δ' , such that, for example, the λ_3 term describes attraction (repulsion) between the order parameters for $\lambda_3 < 0$ ($\lambda_3 > 0$). Note, however, that due to the quadratic nature of this term, such an interaction between the order parameters only amounts to a change of the critical temperature of the secondary order parameter.

B. Comment on three-dimensional ordering

So far, our discussion has been based on a purely two-dimensional model. Despite the layered structure of the kagome metals, it is possible that three-dimensionality is important. Since some experiments report a $2 \times 2 \times 2$ increase in the size of the unit cell [30] and DFT calculations report instabilities at the L -points [31], we are driven to consider L -point charge ordering as well. There are again three inequivalent wavevectors, which in this case are

$$\mathbf{L}_{1,3} = \left(\pm \frac{\pi}{a}, \frac{\pi}{a\sqrt{3}}, \frac{\pi}{c} \right), \quad \mathbf{L}_2 = \left(0, -\frac{2\pi}{a\sqrt{3}}, \frac{\pi}{c} \right), \tag{12}$$

where c is the lattice constant in the vertical direction.

Here, pure L -point third-order terms in the free energy will be absent, since the three momenta do not add up to zero. However, the second- and fourth-order terms will be present and unchanged with respect to the previous case, since only even powers of the order parameters appear and hence the L -point momenta in the z -direction add up to zero. In this sense, the pure L -point *charge* order has the same Landau theory as a pure M -point *flux* order [46]. In the case of the M -point order, it is TRS that forces the absence of a pure third-order term, whereas in the L -point case, it is z -momentum conservation.

In general, if we combine an M -point charge order Δ^M with L -point charge (or flux) order Δ^L (or Δ'^L), then all the allowed third-order terms take the schematic form $\Delta^M (\Delta^L)^2$, $\Delta^M (\Delta'^L)^2$. These terms are only present as long as the M -point order is even under C_2 . Therefore, three-dimensional L -point bond or flux order always induces a subsidiary M -point charge order.

V. PURE BOND ORDER

We start our discussion with pure bond order without any flux order. This case has already been extensively covered in Ref. 31 and here we just summarize the most important results. The possible Landau theories only differ in the presence or absence of the third-order term,

Eq. (9). As can be seen from Tab. III, F_1 and F_2 orders at the M point have a third-order term, while the F_3 and F_4 orders at the M point, as well as any L -point orders lack these terms. Note again that the absence of the third-order term for F_3 and F_4 is an immediate consequence of them being odd under C_2 .

A. Without third-order term

In this case, we have a second-order phase transition, when the coefficient of the quadratic term switches sign, in other words exactly at T_c . The specific form of the ordering is determined by the fourth-order terms. With only Δ present, only the λ_1 and λ_4 fourth-order terms are present. λ_1 alone does not break any degeneracy, irrespective of its value. $\lambda_4 > 0$ then leads to an anisotropic solution immediately below the charge-ordering temperature: Only one of the components Δ_i will be non-zero. On the contrary, $\lambda_4 < 0$ favors an isotropic solution. There are two degenerate isotropic solutions, since the free energy is independent of the sign of the individual order-parameter components: For the F_3 and F_4 irreps, the cases with all components the same sign ($\Delta_1 = \Delta_2 = \Delta_3$) and one component with the opposite sign ($\Delta_1 = -\Delta_2 = -\Delta_3$ or cyclic variations) are degenerate and related by C_2 .

B. With third-order term

In the presence of a third-order term in the free energy, the phase transition changes to first order. Generically, the free energy takes the form

$$\mathcal{F} = \alpha(T - T_c)\Delta^2 + b\Delta^3 + c\Delta^4, \quad (13)$$

which undergoes a first-order transition at $\tilde{T}_c = T_c + b^2/(4\alpha c) > T_c$, where the order parameter jumps to a finite value $\Delta_0 = -\frac{b}{2c}$.

Further, the third-order term lifts the degeneracy between the isotropic solutions. In particular, for $\lambda_4 \leq 0$ and $\beta_1 < 0$, the configuration with $\text{sign}(\Delta_1\Delta_2\Delta_3) > 0$, referred to as tri-hexagonal ordering for the case of F_1 , is favored. When $\beta_1 > 0$, the configuration $\text{sign}(\Delta_1\Delta_2\Delta_3) < 0$, the so-called Star-of-David ordering for F_1 , is favored.

Finally, we can consider the case where $\lambda_4 > 0$ in the presence of a third-order term. In that case, the first-order transition into the $|\Delta_1| = |\Delta_2| = |\Delta_3|$ order is followed by a crossover to $|\Delta_2| = |\Delta_3| \approx 0 < |\Delta_1|$ (or cyclic variations) at lower temperatures.

VI. COUPLED BOND AND FLUX ORDER

We now consider the case, where bond order and flux order coexist. Following our analysis in Sec. III, we only

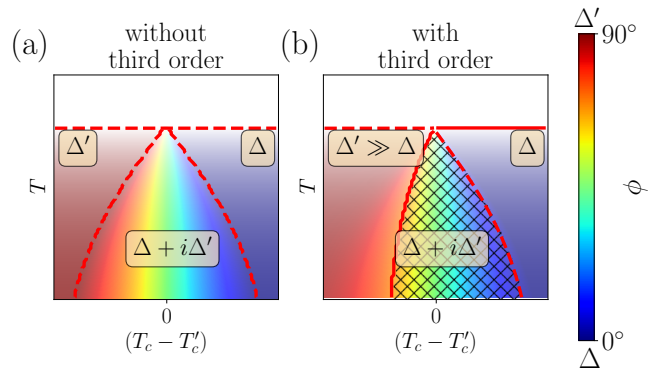


FIG. 3. Phase diagrams (a) without and (b) with third-order terms. The color indicates the angle $\phi = \arctan \frac{\sum_i \Delta'_i{}^2}{\sum_i \Delta_i{}^2}$, while the intensity denotes $\sum_i (\Delta_i^2 + \Delta'_i{}^2)$. Solid lines indicate first-order phase transitions and dashed lines indicate second-order transitions. Hatching denotes an anisotropic solution of the order parameter. TRS is broken when $\Delta' > 0$. The Landau free energy coefficients are chosen to be $\alpha = \alpha' = \lambda_1 = \lambda_2 = \mu_i = \beta_1 = -\beta_2 = 1$, $\lambda_{i>2} = 0$.

have to consider flux orders belonging to the F'_2 and F'_4 irreps, while for bond order, all three-dimensional irreps have to be considered. Translated into our irrep classification, previous work has studied various combinations of bond and flux order parameters: In Ref. 49, the authors study the single order parameter combination F_1 and F'_4 ; Ref. 38 considers the combination F_1 and F'_2 ; Ref. 51 considers F_1 and F'_4 ; and Refs. 50 and 46 consider a variety of different order-parameter combinations.

We construct the free energy \mathcal{F}_{ij} for coupling bond order F_i with flux order F'_j . In the absence of additional perturbations, there are two cases shown in Tab. III: Firstly, we consider coupling bond order that is even under C_2 (from the F_1 or F_2 irreps) to any flux order (from the F'_2 or F'_4 irrep). Then, the free energy

$$\mathcal{F}^{(2)} + \mathcal{F}^{(3,0)} + \mathcal{F}^{(1,2)} + \mathcal{F}^{(4)} \quad (14)$$

includes all third-order terms. Secondly, we consider coupling bond order that is odd under C_2 (from the F_3 or F_4 irreps) to any flux order (from the F'_2 or F'_4 irrep). The corresponding free energy

$$\mathcal{F}^{(2)} + \mathcal{F}^{(4)} \quad (15)$$

consequently has no third-order terms. For both of these two cases, we next present a phase diagram, where we tune the relative strength of the Δ and Δ' order by tuning their relative critical temperature $T_c - T'_c$.

A. Without third-order term

Figure 3a shows the phase diagram without any third-order terms. This is the case, for example, for \mathcal{F}_{34} . Since Δ and Δ' are only coupled via the fourth-order term,

we can have either order parameter existing alone. The phase diagram splits into three ordered regions that are entered through second-order transitions: one where Δ exists alone ($T_c > T \gtrsim T'_c$), one where Δ' exists alone ($T'_c > T \gtrsim T_c$) and one where both coexist. These three regions are separated by second-order phase transitions. As in the case of pure bond order, the fourth-order term can introduce an anisotropy. The terms with coefficients λ_1 , λ_2 and λ_3 do not break the degeneracy between isotropic and anisotropic solutions. $\lambda_4 < 0$ favours an isotropic solution for the bond order, while $\lambda_4 > 0$ favours an anisotropic solution. λ_5 plays the same role for the flux order. $\lambda_6 > 0$ may also introduce anisotropy, but this term is only active if both bond and flux order are present. TRS is broken any time Δ' is non-zero. Note that without a third-order term, there is a symmetry under exchanging Δ and Δ' (as well as exchanging the corresponding coefficients of the free energy). This explains the left-right symmetry in the phase diagram.

B. With third-order term

Figure 3b shows the phase diagram with third-order terms, such as the free energy \mathcal{F}_{12} . In this case, a finite Δ' always induces a subsidiary Δ . Unlike the case without third-order terms, where there are three regions and the phase-transition into the coexistence region happens at a singular point ($T_c = T'_c$) and is always second order, here the phase diagram only has two regions: one, where Δ appears alone and TRS is preserved and one, where both order parameters coexist and TRS is broken. As in the pure bond-order case, the transition into the former is always first order with a (potential) additional second-order transition into the coexistence region. The direct transition into the coexistence region changes from first order for $T_c \approx T'_c$ and $\Delta' \sim \Delta$ to second order for $T'_c \gg T_c$ and $\Delta' \gg \Delta$. Within the ordered phase, there is then a crossover between these domains. More details on the transitions can be found in appendix D.

Further, the third-order term can induce anisotropy even when the fourth-order term prefers an isotropic solution ($\lambda_n = 0$ for $n > 3$). For $\Delta' = 0$, the solutions are isotropic, but when $\Delta' \neq 0$, we can have an anisotropic solution with $|\Delta_i| \neq |\Delta_j|$ for some i, j , if the order parameter is large enough for the third-order term to be relevant. Finally, the third-order term now breaks the symmetry of exchanging Δ and Δ' , such that the phase diagram is no longer left-right symmetric.

VII. SYMMETRY-BREAKING

A. Coupling to strain

Uniaxial strain has proven to be a very effective perturbation to probe correlated orders in two-dimensional and layered materials. Uniaxial strain was used in layered

systems such as the cuprates to probe the charge density wave [53] or Sr_2RuO_4 [54], where it lifts the degeneracy of critical temperatures for the superconducting and TRS-breaking states, while the ground state in twisted bilayer graphene changes drastically under strain [55]. Indeed, recent experiments indicate that coupling to strain significantly alters the transport properties of kagome metals [24] and we therefore include such coupling in our Landau theory. The strain matrix in terms of the displacement field \mathbf{u} is given by $\epsilon_{\alpha\beta} = \frac{1}{2}(\partial_\alpha u_\beta + \partial_\beta u_\alpha)$. The coupling to strain is independent of the order parameters we consider and has the form (see appendix C)

$$\begin{aligned} \mathcal{F}^{(\text{str})} = & \mu_2 [(\epsilon_{xx} - \epsilon_{yy})(\Delta_1^2 - \Delta_2^2/2 - \Delta_3^2/2) \\ & + \epsilon_{xy}\sqrt{3}(\Delta_2^2 - \Delta_3^2)] \\ & + \mu_3 [(\epsilon_{xx} - \epsilon_{yy})(\Delta_1'^2 - \Delta_2'^2/2 - \Delta_3'^2/2) \\ & + \epsilon_{xy}\sqrt{3}(\Delta_2'^2 - \Delta_3'^2)]. \end{aligned} \quad (16)$$

Being quadratic in the order parameters, strain shifts the critical temperatures of different components of the order parameters and as such, it is possible that strain induces an order even though the temperature is too high in the strainless state. For example, it is possible for the strain to increase the critical temperature of one of the components of the flux order and thereby break TRS.

Finally, we note that having a first-order transition relies on the third-order term being relevant. The presence of strain favors some of the components of Δ over others and, therefore, weakens the effect of the third-order term $\Delta_1\Delta_2\Delta_3$. Strain thus generally weakens the first-order nature of the transition into the ordered state.

B. Anisotropy

As anisotropy we denote the breaking of rotation symmetry in a system. In the context of crystalline systems, where rotation symmetry is already discrete, anisotropy then refers to a further reduction, such as the breaking of C_6 down to C_2 . In the context of a charge-density-wave instability with multiple inequivalent wave vectors, an anisotropy can arise from different magnitudes of the individual order-parameter components. Note that in the following, we consider purely in-plane order, since for finite out-of-plane momentum (such as L -point ordering), the rotational symmetry can be trivially broken [31].

Strain explicitly breaks rotation symmetry and will thus introduce an anisotropy. The susceptibility towards an anisotropy in a small strain field can thus serve as an indicator for the anisotropy in the system. In particular, the susceptibility of a C_3 -breaking order parameter to strain will diverge for an anisotropic ground state. We thus calculate $\{\Delta_1^2 - \Delta_2^2/2 - \Delta_3^2/2, \frac{\sqrt{3}}{2}(\Delta_2^2 - \Delta_3^2)\}$ to assess whether rotational symmetry is broken and, similarly, for the corresponding order parameter for flux order. In appendix C, we show how the susceptibility is related to this 'order parameter' $\sum_{i,j} [(\Delta_i^2 - \Delta_j^2)^2 + (\Delta_i'^2 - \Delta_j'^2)^2]$.

Below, we discuss the conditions for an anisotropy in the solution to the Landau free energy in the cases without and with third-order terms.

1. Without third-order term

As shown in Sec. V A, pure bond order is anisotropic when the fourth-order term $\lambda_4 > 0$. Similarly, flux order is anisotropic when $\lambda_5 > 0$. In addition, $\lambda_6 > 0$ leads to an anisotropic solution, if both bond and flux order are non-zero. Note that the non-zero component of the two orders is the same, meaning a solution of the form $\Delta_i \neq 0$, $\Delta'_i \neq 0$ is stable.

2. With third-order term

Anisotropy can arise from the third-order term in the free energy even when the fourth-order terms favor an isotropic solution. To see this, consider the terms

$$\beta_1 \Delta_1 \Delta_2 \Delta_3 + \beta_2 (\Delta_1 \Delta'_2 \Delta'_3 + \Delta'_1 \Delta_2 \Delta'_3 + \Delta'_1 \Delta'_2 \Delta_3) \quad (17)$$

as perturbations with $\Delta^2 = \Delta_1^2 + \Delta_2^2 + \Delta_3^2$ and $\Delta'^2 = \Delta_1'^2 + \Delta_2'^2 + \Delta_3'^2$ being fixed by the second order and fourth order terms in the free energy. Let us assume $\beta_1 > 0$ and $\beta_2 < 0$ (the case $\beta_1 < 0$ and $\beta_2 > 0$ can be obtained by flipping the sign of Δ_i). We can then compare the energies of two extreme cases: For an isotropic solution $\Delta_1 = \Delta_2 = \Delta_3 = \Delta/\sqrt{3}$ and $\Delta'_1 = \Delta'_2 = \Delta'_3 = \Delta'/\sqrt{3}$, the third order terms yield an energy

$$\frac{|\beta_1|}{3\sqrt{3}} \Delta^3 - \frac{|\beta_2|}{3\sqrt{3}} \Delta \Delta'^2 \quad (18)$$

while the anisotropic solution $\Delta_1 = \Delta$ and $\Delta'_2 = \Delta'_3 = \Delta'/\sqrt{2}$ has energy

$$-\frac{|\beta_2|}{2} \Delta \Delta'^2. \quad (19)$$

Therefore the isotropic solution will be favoured when $(\Delta'/\Delta)^2 > (\frac{3\sqrt{3}}{2} - 1)|\beta_1|/|\beta_2|$. Increasing the ratio Δ'/Δ corresponds to moving to the left in the phase diagram of Figure 3b. Similarly, the anisotropic solution gives way to an isotropic solution when Δ is large (see appendix E for details). This leads to the wedge-shaped region in the phase diagram where the solution is anisotropic.

C. Coupling to a z-axis magnetic field

The lowest-order coupling to a magnetic field is linear in field and quadratic in the order parameters. However, only some of the order-parameter combinations couple to a magnetic field at this lowest order. The magnetic field breaks TRS and transforms under the A_2 irrep of C_{6v}''' . Therefore, for the order parameters to couple in this

manner to the magnetic field, we require $A_2 \subset F_i \otimes F'_j$. If the coupling is allowed (see Tab. III), it takes the form

$$\mathcal{F}^{(B)} = \mu_1 B (\Delta_1 \Delta'_1 + \Delta_2 \Delta'_2 + \Delta_3 \Delta'_3). \quad (20)$$

We note that this is an unusual form of magnetic field coupling to (translational-symmetry-breaking) order parameters since the magnetic field couples *linearly*. This is only possible since we have both TRS-breaking and TRS-preserving orders with the same wavevectors. Importantly, this term fixes the relative sign between Δ and Δ' . Without a magnetic field, there can be domains with opposite relative signs. Applying a magnetic field causes the domains to flip such that the relative sign is the same everywhere. We note in passing that this form of the coupling to the magnetic field would also be possible if Δ and Δ' are both L -point orders, but not for a combination of an L -point and M -point order.

1. Without third-order term

Figure 4a shows the phase diagram in the presence of a magnetic field, when there is no third-order terms in the free energy. The only order-parameter combination that has the lowest-order coupling to a magnetic field, while lacking a third-order term, is F_3 with F'_4 , in other words the free energy \mathcal{F}_{34} . In this case, the magnetic field couples Δ and Δ' and hence, the two orders always coexist. The regions $\Delta \gg \Delta'$, $\Delta \sim \Delta'$, and $\Delta \ll \Delta'$ are now separated by crossovers. In the region $T_c \sim T'_c$, the critical temperature is enhanced as both order parameters condense at the same time. While TRS is trivially broken in the entire phase diagram, the magnetic field does not induce an anisotropy if not present already. Note that while in Ref. 56 the effect of magnetic field in a Landau theory of the kagome metals was considered, only the case without third-order terms was treated.

2. With third-order term

Figure 4b, finally, shows the phase diagram in the presence of a magnetic field, when there is a third-order term in the free energy. The only order parameter combination that has both the lowest-order coupling to a magnetic field and a third-order term is F_1 with F'_2 , in other words the free energy \mathcal{F}_{12} . The two order parameters are again coupled and always appear together. The regions $\Delta \gg \Delta'$, $\Delta \sim \Delta'$, and $\Delta \ll \Delta'$ are separated by crossovers. Due to the third-order term, an anisotropy can be induced, if Δ and Δ' both become large enough. In the region where $T_c > T'_c$, adding the magnetic field increases the strength of the flux order, thereby enhancing the anisotropy via the third-order term. This is shown explicitly in appendix F. Again, TRS is trivially broken in the entire phase diagram.

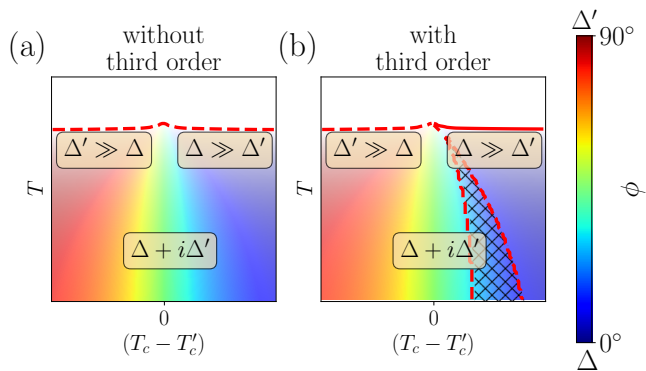


FIG. 4. Phase diagrams in the presence of a magnetic field (a) without and (b) with third-order terms in the free energy. The color indicates the angle $\phi = \arctan \frac{\sum_i \Delta'_i{}^2}{\sum_i \Delta_i{}^2}$, while the intensity denotes $\sum_i (\Delta_i^2 + \Delta'_i{}^2)$. Solid lines indicate first-order phase transitions and dashed lines indicate second-order transitions. Hatching denotes an anisotropic solution of the order parameter. TRS is broken everywhere due to the applied field. The Landau free energy coefficients are chosen to be $\alpha = \alpha' = \lambda_1 = \lambda_2 = \mu_i = \beta_1 = -\beta_2 = 1$, $\lambda_{i>2} = 0$.

VIII. CONSTRAINTS FROM EXPERIMENTS ON AV_3Sb_5

While our phenomenological description of charge density orders in kagome metals is valid for any such system, we comment in the following on the consequences of our discussion for the AV_3Sb_5 family. There are several experimental facts, which any theory of the charge-ordered (normal) state should reproduce:

1. A 2×2 increase in the in-plane unit cell at T_c as observed by X-ray diffraction [6, 30, 43] and STM [8, 9, 11, 44].
2. The transition at T_c appears to be first order. First, the heat capacity displays a sharp peak at T_c [6], which is a general feature of a first-order transition. In addition, X-ray scattering [30] and NMR [57] show discontinuities at T_c , further suggesting a first-order transition. Finally, transport [19, 24] does not see an extended region of fluctuations but a rather abrupt change, especially for out-of-plane conductivity.
3. TRS is/can be broken below $T' < T_c$, as seen in muon spin-relaxation [16, 26] and Kerr rotation [17, 27]. It is currently uncertain whether this is truly spontaneous TRSB or whether it is a giant response to a small applied magnetic field. In either case, it is clear that the coupling of the order to (out-of-plane) magnetic fields is important: A small field leads to a giant anomalous Hall response [32, 33] and a large μSR response [16, 58, 59]. Finally, such a magnetic field (linearly) couples the chirality of the ordered state [22].

Experimental fact 1 implies we should consider the translational-symmetry breaking orders of C_{6v}''' , in other words the four three-dimensional irreps denoted as F_i , $i = 1, \dots, 4$. Experimental fact 2 requires the presence of a third-order term in \mathcal{F} . Absent a third-order term, the phase-transitions in the Landau free energy are generically second order. Experimental fact 3 suggests that the system is at least very tunable towards TRSB order, which should therefore lie close in energy to the ground state. This implies we should consider additional flux order, in other words F'_2 and F'_4 . In addition, experimental fact 3 requires a term that (linearly) couples the magnetic field to the order parameters. In our classification, the only order-parameter combination that has third-order terms as well as (linear) coupling to a magnetic field is F_1 with F'_2 . There is evidence from experiments and density functional theory that the charge order transforms as the F_1 irrep [60–64], which supports the conclusion reached above using different means. The nature of the flux order has not been determined yet by other means.

IX. PROPOSALS FOR FUTURE EXPERIMENTS ON AV_3Sb_5

A. Transport

With the order parameter combination F_1 and F'_2 we are able to explain the striking experimental results seen in transport in Ref. [24]. The experiment reported isotropic transport in the absence of strain, however application of an *out-of-plane* magnetic field leads to anisotropic transport. If we are in the regime where $T_c \gg T'_c$, then only Δ is induced at T_c and this order is isotropic. However, a magnetic field will induce Δ' at T_c as well (due to the μ_1 term in the free energy). The β_2 third-order term coupling Δ and Δ' can then lead to anisotropy as outlined in Sec. VIII B.

One natural future direction to explore is how closely the transport anisotropy is related to the charge order. It has been shown that with sufficient Nb and Ta doping on the V-site, the chemical pressure can suppress the charge density wave transition down to lower or even zero temperature [65, 66]. The report of an isotropic superconducting gap suggests the absence of anisotropy without applying an external field [67], but the field- or strain-induced anisotropy is yet to be explored. Therefore, we propose a complete mapping of anisotropy across the doping phase diagram in order to explore how the field- and strain- dependence of the electronic anisotropy evolves when the charge order is suppressed or absent.

Meanwhile, previous experimental results showed that when a magnetic field is applied, the direction of transport anisotropy seems to be pinned to a particular direction most likely due to the small uniaxial strain [24]. It is worth checking whether this pinning can be altered by a strong current pulse which may overcome the barrier of the pinning energy.

Moreover, the angular dependence of magnetoresistance (MR) seems to suggest a two-fold symmetry which indicates a breaking of the six-fold in plane rotation symmetry [21]. Yet, this technique is strongly limited by the misalignment of the magnetic field direction due to the huge magnetoresistance spike with in-plane field [22]. Therefore, measuring the angular dependence of the magnetoresistance with a spherical rotation of the magnetic field direction would reveal the true in-plane component of MR with and without an out-of-plane field component.

Furthermore, we are working with the assumption that there is no anisotropy in the strain-free case. Elastoresistance measurements such as those in Ref. 10 are interesting in order to quantify the dependence on strain.

Most of the theoretical treatment of our work assumes a two-dimensional nature of the charge ordering. One important open question is how much of the physics of the charge density order is two-dimensional. In particular, a possible explanation of the data in Ref. 24 observing isotropic transport is that while the transport in a given layer is anisotropic, the transport averages over different layers such that one obtains isotropic transport. In order to rule out this scenario, one could probe the transport in a two-dimensional film of the material. Indeed, there has been recent progress in manufacturing thin films of the kagome metals via exfoliation [68–70]. It would be exciting to reach the monolayer limit and measure transport anisotropy in that case.

B. STM

Another approach to detect whether the isotropic transport behaviour in the low strain devices of Ref. 24 arises due to averaging over many domains/layers would be to perform local measurements of the anisotropy, for example via STM, on ultra-low strain devices. Reference 24 reports anisotropic transport once a magnetic field is switched on. It would be interesting to perform an STM study (or indeed an X-ray scattering experiment) when the sample is in a magnetic field, in order to establish the source of this anisotropy. However, one should caution that STM is a surface probe and the physics probed at the surface may not necessarily be representative of the physics in the bulk.

C. TRSB

Currently the results on TRSB in Kagome metals are still controversial, in particular, there is no consensus on whether there is spontaneous TRSB in zero magnetic field or whether the TRSB is induced by the small training fields used in experiments. In terms of the probes used to investigate (spontaneous) TRSB in the Kagome metals, there have been both Kerr effect and muon spin rotation experiments. Another probe that could be used to detect the circulating currents predicted in these ma-

terials is neutron scattering. This technique has been successfully used to detect the loop currents in the pseudogap phase of the cuprates [71].

Our Landau theory as well as recent experiments [24] show that kagome metals can be very sensitive to strain. While these experiments showed that there was no observable dependence of the charge-ordering temperature on the strain, it has yet to be established whether the TRSB temperature depends on strain.

D. Stiffness measurements

Transport experiments have revealed that the anisotropy in strain-free samples increases when a magnetic field is applied and this should yield observable signatures in measurements of elements of the stiffness matrix, as we elaborate on below.

In addition to the coupling between the strain and the order parameters, there is also a contribution to the free energy coming from the elastic energy itself. Using the Voigt notation for the strain tensor, i.e., introducing the six-dimensional vector $\epsilon = (\epsilon_{xx}, \epsilon_{yy}, \epsilon_{zz}, 2\epsilon_{yz}, 2\epsilon_{xz}, 2\epsilon_{xy})$, we can write the elastic energy as

$$\mathcal{F}(\epsilon) = \frac{1}{2} \sum_{\alpha\beta} c_{\alpha\beta} \epsilon_{\alpha} \epsilon_{\beta}, \quad (21)$$

where $c_{\alpha\beta}$ is the stiffness matrix. For a system with D_{6h} symmetry, there are five independent components of the stiffness matrix [50]: $c_{11}, c_{12}, c_{13}, c_{33}, c_{44}$. In general, the components of the stiffness matrix can be discontinuous at a second-order phase transition, which can be measured in experiments. The discontinuities are given by the formula [50, 72, 73]

$$\Delta c_{\alpha\beta} = \sum_{\gamma\delta} \frac{\partial^2 \mathcal{F}(\text{str})}{\partial \epsilon_{\alpha} \partial D_{\gamma}} \frac{\partial^2 \mathcal{F}(\text{str})}{\partial \epsilon_{\beta} \partial D_{\delta}} \left(\frac{\partial^2 \mathcal{F}}{\partial D_{\gamma} \partial D_{\delta}} \right)^{-1}, \quad (22)$$

where $\mathbf{D} = (\Delta, \Delta')$ is the six-dimensional vector combining the order parameters. As shown in Ref. 50, at the onset of isotropic charge ordering, there will be discontinuities $\Delta c_{11}, \Delta c_{12}, \Delta c_{13}, \Delta c_{33}$. On the other hand, at the onset of anisotropic order, there will be further independent components of the stiffness matrix, which are discontinuous, namely $\Delta c_{22} \neq \Delta c_{11}$ and $\Delta c_{13} \neq \Delta c_{23}$. Therefore, one interesting experiment would be to measure $\Delta c_{22} - \Delta c_{11}$ and $\Delta c_{13} - \Delta c_{23}$ in a pristine (strain-free) sample as a function of an applied magnetic field.

Resonant ultrasound spectroscopy is a method used to measure the elements of the elastic stiffness matrix [74]. It would be interesting to perform these experiments as a function of the applied magnetic field, though resonant ultrasound spectroscopy in a magnetic field is challenging and it is possible that pulse-echo sound velocity measurements are more realistic.

X. CONCLUSION

Kagome metals are known to undergo charge ordering with a 2×2 increase in the size of the unit cell. Using a group theory analysis, we write down all possible site, bond and flux ordering that is consistent with the system symmetries. The observation of TRSB and coupling to a magnetic field further motivates studying TRSB flux order. Flux and bond order are natural partners since they are the imaginary and real part of the same underlying order parameter and so in general, we expect these two orders to be coupled. This leads us to study *all* possibilities for the coupling of flux and bond order.

We use a Landau analysis to study the interplay of the two orders. The different types of flux and bond order lead to differences in the third order term in the Landau theory as well as differences in the coupling to the magnetic field. We construct the phase diagrams for different types of coupled flux and bond order. Depending on the type of order, the two order parameters corresponding to flux and bond order may appear separately or always in

unison.

By synthesizing various experimental results and comparing to the Landau theory phase diagrams, we are able to deduce that the most likely candidate is a trihexagonal or Star of David bond order with a subsidiary C_2 -preserving flux order.

XI. ACKNOWLEDGEMENTS

We thank F. Grandi and M. Christensen for comments on a previous version of the manuscript. We also thank R. Fernandes for helpful discussions. This project was supported by the European Research Council (ERC) under the European Union's Horizon 2020 research and innovation program grant nos. ERC-StG-Neupert-757867-PARATOP (GW, TN) and 715730 (CG, PJWM). TN acknowledges funding from the Swiss National Science Foundation (Project 200021E 198011) as part of the QUAST FOR 5249-449872909 (Project P3).

-
- [1] Aron J. Beekman, Louk Rademaker, and Jasper van Wezel. An introduction to spontaneous symmetry breaking. *SciPost Phys. Lect. Notes*, page 11, 2019. doi:10.21468/SciPostPhysLectNotes.11. URL <https://scipost.org/10.21468/SciPostPhysLectNotes.11>.
- [2] Catherine Kallin and John Berlinsky. Chiral superconductors. *Reports on Progress in Physics*, 79(5):054502, apr 2016. doi:10.1088/0034-4885/79/5/054502. URL <https://dx.doi.org/10.1088/0034-4885/79/5/054502>.
- [3] W. D. Wise, M. C. Boyer, Kamallesh Chatterjee, Takeshi Kondo, T. Takeuchi, H. Ikuta, Yayu Wang, and E. W. Hudson. Charge-density-wave origin of cuprate checkerboard visualized by scanning tunnelling microscopy. *Nature Physics*, 4(9):696–699, 2008. doi:10.1038/nphys1021. URL <https://doi.org/10.1038/nphys1021>.
- [4] Titus Neupert, M. Michael Denner, Jia-Xin Yin, Ronny Thomale, and M. Zahid Hasan. Charge order and superconductivity in kagome materials. *Nature Physics*, 18(2):137–143, 2022. doi:10.1038/s41567-021-01404-y. URL <https://doi.org/10.1038/s41567-021-01404-y>.
- [5] Thanh Nguyen and Mingda Li. Electronic properties of correlated kagome metals AV_3Sb_5 : A perspective. *Journal of Applied Physics*, 131(6):060901, 2022. doi:10.1063/5.0079593. URL <https://doi.org/10.1063/5.0079593>.
- [6] Brenden R. Ortiz, Samuel M. L. Teicher, Yong Hu, Julia L. Zuo, Paul M. Sarte, Emily C. Schueller, A. M. Milinda Abeykoon, Matthew J. Krogstad, Stephan Rosenkranz, Raymond Osborn, Ram Seshadri, Leon Balents, Junfeng He, and Stephen D. Wilson. CsV_3Sb_5 : A Z_2 topological kagome metal with a superconducting ground state. *Phys. Rev. Lett.*, 125:247002, Dec 2020. doi:10.1103/PhysRevLett.125.247002. URL <https://link.aps.org/doi/10.1103/PhysRevLett.125.247002>.
- [7] Hongen Zhu, Tongrui Li, Fanghang Yu, Yuliang Li, Sheng Wang, Yunbo Wu, Zhanfeng Liu, Zhengming Shang, Shengtao Cui, Yi Liu, Guobin Zhang, Lidong Zhang, Zhenyu Wang, Tao Wu, Jianjun Ying, Xianhui Chen, and Zhe Sun. Electronic instability of kagome metal CsV_3Sb_5 in the $2 \times 2 \times 2$ charge density wave state. *Chinese Physics Letters*, 2023. URL <http://iopscience.iop.org/article/10.1088/0256-307X/40/4/047301>.
- [8] He Zhao, Hong Li, Brenden R. Ortiz, Samuel M. L. Teicher, Takamori Park, Mengxing Ye, Ziqiang Wang, Leon Balents, Stephen D. Wilson, and Ilija Zeljkovic. Cascade of correlated electron states in the kagome superconductor CsV_3Sb_5 . *Nature*, 599(7884):216–221, 2021. doi:10.1038/s41586-021-03946-w. URL <https://doi.org/10.1038/s41586-021-03946-w>.
- [9] Hui Chen, Haitao Yang, Bin Hu, Zhen Zhao, Jie Yuan, Yuqing Xing, Guojian Qian, Zihao Huang, Geng Li, Yuhan Ye, Sheng Ma, Shunli Ni, Hua Zhang, Qiangwei Yin, Chunsheng Gong, Zhijun Tu, Hechang Lei, Hengxin Tan, Sen Zhou, Chengmin Shen, Xiaoli Dong, Binghai Yan, Ziqiang Wang, and Hong-Jun Gao. Roton pair density wave in a strong-coupling kagome superconductor. *Nature*, 599(7884):222–228, 2021. doi:10.1038/s41586-021-03983-5. URL <https://doi.org/10.1038/s41586-021-03983-5>.
- [10] Linpeng Nie, Kuanglv Sun, Wanru Ma, Dianwu Song, Lixuan Zheng, Zuwei Liang, Ping Wu, Fanghang Yu, Jian Li, Min Shan, Dan Zhao, Shunjiao Li, Baolei Kang, Zhimian Wu, Yanbing Zhou, Kai Liu, Ziji Xiang, Jianjun Ying, Zhenyu Wang, Tao Wu, and Xianhui Chen. Charge-density-wave-driven electronic nematicity in a kagome superconductor. *Nature*, 604(7904):59–64, 2022. doi:10.1038/s41586-022-04493-8. URL <https://doi.org/10.1038/s41586-022-04493-8>.
- [11] Yu-Xiao Jiang, Jia-Xin Yin, M. Michael Denner, Nana Shumiya, Brenden R. Ortiz, Gang Xu, Zurab Guguchia,

- Junyi He, Md Shafayat Hossain, Xiaoxiong Liu, Jacob Ruff, Linus Kautzsch, Songtian S. Zhang, Guoqing Chang, Ilya Belopolski, Qi Zhang, Tyler A. Cochran, Daniel Multer, Maksim Litskevich, Zi-Jia Cheng, Xian P. Yang, Ziqiang Wang, Ronny Thomale, Titus Neupert, Stephen D. Wilson, and M. Zahid Hasan. Unconventional chiral charge order in kagome superconductor KV_3Sb_5 . *Nature Materials*, 20(10):1353–1357, 2021. doi: 10.1038/s41563-021-01034-y. URL <https://doi.org/10.1038/s41563-021-01034-y>.
- [12] Hong Li, He Zhao, Brenden R. Ortiz, Takamori Park, Mengxing Ye, Leon Balents, Ziqiang Wang, Stephen D. Wilson, and Ilija Zeljkovic. Rotation symmetry breaking in the normal state of a kagome superconductor KV_3Sb_5 . *Nature Physics*, 18(3):265–270, 2022. doi: 10.1038/s41567-021-01479-7. URL <https://doi.org/10.1038/s41567-021-01479-7>.
- [13] D. W. Song, L. X. Zheng, F. H. Yu, J. Li, L. P. Nie, M. Shan, D. Zhao, S. J. Li, B. L. Kang, Z. M. Wu, Y. B. Zhou, K. L. Sun, K. Liu, X. G. Luo, Z. Y. Wang, J. J. Ying, X. G. Wan, T. Wu, and X. H. Chen. Orbital ordering and fluctuations in a kagome superconductor CsV_3Sb_5 , 2021.
- [14] Lixuan Zheng, Zhimian Wu, Ye Yang, Linpeng Nie, Min Shan, Kuanglv Sun, Dianwu Song, Fanghang Yu, Jian Li, Dan Zhao, Shunjiao Li, Baolei Kang, Yanbing Zhou, Kai Liu, Ziji Xiang, Jianjun Ying, Zhenyu Wang, Tao Wu, and Xianhui Chen. Emergent charge order in pressurized kagome superconductor CsV_3Sb_5 . *Nature*, 611(7937):682–687, 2022. doi:10.1038/s41586-022-05351-3. URL <https://doi.org/10.1038/s41586-022-05351-3>.
- [15] Q. Chen, D. Chen, W. Schnelle, C. Felser, and B. D. Gaulin. Charge density wave order and fluctuations above T_{cdw} and below superconducting T_c in the kagome metal CsV_3Sb_5 . *Phys. Rev. Lett.*, 129:056401, Jul 2022. doi:10.1103/PhysRevLett.129.056401. URL <https://link.aps.org/doi/10.1103/PhysRevLett.129.056401>.
- [16] C. Mielke, D. Das, J. X. Yin, H. Liu, R. Gupta, Y. X. Jiang, M. Medarde, X. Wu, H. C. Lei, J. Chang, Pengcheng Dai, Q. Si, H. Miao, R. Thomale, T. Neupert, Y. Shi, R. Khasanov, M. Z. Hasan, H. Luetkens, and Z. Guguchia. Time-reversal symmetry-breaking charge order in a kagome superconductor. *Nature*, 602(7896):245–250, 2022. doi:10.1038/s41586-021-04327-z. URL <https://doi.org/10.1038/s41586-021-04327-z>.
- [17] Li Yu, Chennan Wang, Yuhang Zhang, Mathias Sander, Shunli Ni, Zouyouwei Lu, Sheng Ma, Zhengguo Wang, Zhen Zhao, Hui Chen, Kun Jiang, Yan Zhang, Haitao Yang, Fang Zhou, Xiaoli Dong, Steven L. Johnson, Michael J. Graf, Jiangping Hu, Hong-Jun Gao, and Zhongxian Zhao. Evidence of a hidden flux phase in the topological kagome metal CsV_3Sb_5 , 2021.
- [18] C. C. Zhao, L. S. Wang, W. Xia, Q. W. Yin, J. M. Ni, Y. Y. Huang, C. P. Tu, Z. C. Tao, Z. J. Tu, C. S. Gong, H. C. Lei, Y. F. Guo, X. F. Yang, and S. Y. Li. Nodal superconductivity and superconducting domes in the topological kagome metal CsV_3Sb_5 , 2021.
- [19] Brenden R. Ortiz, Lídia C. Gomes, Jennifer R. Morey, Michal Winiarski, Mitchell Bordelon, John S. Mangum, Iain W. H. Oswald, Jose A. Rodriguez-Rivera, James R. Neilson, Stephen D. Wilson, Elif Ertekin, Tyrel M. McQueen, and Eric S. Toberer. New kagome prototype materials: discovery of KV_3Sb_5 , RbV_3Sb_5 , and CsV_3Sb_5 . *Phys. Rev. Mater.*, 3:094407, Sep 2019. doi:10.1103/PhysRevMaterials.3.094407. URL <https://link.aps.org/doi/10.1103/PhysRevMaterials.3.094407>.
- [20] Feng Du, Shuaishuai Luo, Brenden R. Ortiz, Ye Chen, Weiyan Duan, Dongting Zhang, Xin Lu, Stephen D. Wilson, Yu Song, and Huiqiu Yuan. Pressure-induced double superconducting domes and charge instability in the kagome metal KV_3Sb_5 . *Phys. Rev. B*, 103:L220504, Jun 2021. doi:10.1103/PhysRevB.103.L220504. URL <https://link.aps.org/doi/10.1103/PhysRevB.103.L220504>.
- [21] Ying Xiang, Qing Li, Yongkai Li, Wei Xie, Huan Yang, Zhiwei Wang, Yugui Yao, and Hai-Hu Wen. Twofold symmetry of c-axis resistivity in topological kagome superconductor CsV_3Sb_5 with in-plane rotating magnetic field. *Nature Communications*, 12(1):6727, 2021. doi: 10.1038/s41467-021-27084-z. URL <https://doi.org/10.1038/s41467-021-27084-z>.
- [22] Chunyu Guo, Carsten Putzke, Sofia Konyzheva, Xiangwei Huang, Martin Gutierrez-Amigo, Ion Errea, Dong Chen, Maia G. Vergniory, Claudia Felser, Mark H. Fischer, Titus Neupert, and Philip J. W. Moll. Switchable chiral transport in charge-ordered kagome metal CsV_3Sb_5 . *Nature*, 611(7936):461–466, 2022. doi: 10.1038/s41586-022-05127-9. URL <https://doi.org/10.1038/s41586-022-05127-9>.
- [23] Xiangwei Huang, Chunyu Guo, Carsten Putzke, Martin Gutierrez-Amigo, Yan Sun, Maia G. Vergniory, Ion Errea, Dong Chen, Claudia Felser, and Philip J. W. Moll. Three-dimensional fermi surfaces from charge order in layered CsV_3Sb_5 . *Phys. Rev. B*, 106:064510, Aug 2022. doi:10.1103/PhysRevB.106.064510. URL <https://link.aps.org/doi/10.1103/PhysRevB.106.064510>.
- [24] Chunyu Guo, Glenn Wagner, Carsten Putzke, Dong Chen, Kaize Wang, Ling Zhang, Martin Gutierrez-Amigo, Ion Errea, Maia G. Vergniory, Claudia Felser, Mark H. Fischer, Titus Neupert, and Philip J. W. Moll. Correlated order at the tipping point in the kagome metal CsV_3Sb_5 , 2023.
- [25] Chunyu Guo, Maarten R. van Delft, Martin Gutierrez-Amigo, Dong Chen, Carsten Putzke, Glenn Wagner, Mark H. Fischer, Titus Neupert, Ion Errea, Maia G. Vergniory, Steffen Wiedmann, Claudia Felser, and Philip J. W. Moll. Distinct switching of chiral transport in the kagome metals KV_3Sb_5 and CsV_3Sb_5 , 2023.
- [26] Yajian Hu, Soichiro Yamane, Giordano Mattoni, Kanae Yada, Keito Obata, Yongkai Li, Yugui Yao, Zhiwei Wang, Jingyuan Wang, Camron Farhang, Jing Xia, Yoshiteru Maeno, and Shingo Yonezawa. Time-reversal symmetry breaking in charge density wave of CsV_3Sb_5 detected by polar Kerr effect, 2023.
- [27] Yishuai Xu, Zhuoliang Ni, Yizhou Liu, Brenden R. Ortiz, Qinwen Deng, Stephen D. Wilson, Binghai Yan, Leon Balents, and Liang Wu. Three-state nematicity and magneto-optical Kerr effect in the charge density waves in kagome superconductors. *Nature Physics*, 18(12):1470–1475, 2022. doi:10.1038/s41567-022-01805-7. URL <https://doi.org/10.1038/s41567-022-01805-7>.
- [28] David R. Saykin, Camron Farhang, Erik D. Kountz, Dong Chen, Brenden R. Ortiz, Chandra Shekhar, Claudia Felser, Stephen D. Wilson, Ronny Thomale, Jing Xia, and Aharon Kapitulnik. High resolution polar Kerr effect studies of CsV_3Sb_5 : Tests for time reversal symmetry breaking below the charge order transition, 2022.

- [29] Camron Farhang, Jingyuan Wang, Brenden R. Ortiz, Stephen D. Wilson, and Jing Xia. Unconventional optical rotation in the charge ordered state of kagome metal CsV_3Sb_5 , 2023.
- [30] Haoxiang Li, G. Fabbris, A. H. Said, J. P. Sun, Yu-Xiao Jiang, J. X. Yin, Yun-Yi Pai, Sangmoon Yoon, Andrew R. Lupini, C. S. Nelson, Q. W. Yin, C. S. Gong, Z. J. Tu, H. C. Lei, J. G. Cheng, M. Z. Hasan, Ziqiang Wang, Binghai Yan, R. Thomale, H. N. Lee, and H. Miao. Discovery of conjoined charge density waves in the kagome superconductor CsV_3Sb_5 . *Nature Communications*, 13(1):6348, 2022. doi:10.1038/s41467-022-33995-2. URL <https://doi.org/10.1038/s41467-022-33995-2>.
- [31] Morten H. Christensen, Turan Birol, Brian M. Andersen, and Rafael M. Fernandes. Theory of the charge density wave in AV_3Sb_5 kagome metals. *Phys. Rev. B*, 104:214513, Dec 2021. doi:10.1103/PhysRevB.104.214513. URL <https://link.aps.org/doi/10.1103/PhysRevB.104.214513>.
- [32] Shuo-Ying Yang, Yaojia Wang, Brenden R. Ortiz, Defa Liu, Jacob Gayles, Elena Derunova, Rafael Gonzalez-Hernandez, Libor Šmejkal, Yulin Chen, Stuart S. P. Parkin, Stephen D. Wilson, Eric S. Toberer, Tyrel McQueen, and Mazhar N. Ali. Giant, unconventional anomalous Hall effect in the metallic frustrated magnet candidate, KV_3Sb_5 . *Science Advances*, 6(31):eabb6003, 2020. doi:10.1126/sciadv.abb6003. URL <https://www.science.org/doi/abs/10.1126/sciadv.abb6003>.
- [33] F. H. Yu, T. Wu, Z. Y. Wang, B. Lei, W. Z. Zhuo, J. J. Ying, and X. H. Chen. Concurrence of anomalous Hall effect and charge density wave in a superconducting topological kagome metal. *Phys. Rev. B*, 104:L041103, Jul 2021. doi:10.1103/PhysRevB.104.L041103. URL <https://link.aps.org/doi/10.1103/PhysRevB.104.L041103>.
- [34] Zhiwei Wang, Yu-Xiao Jiang, Jia-Xin Yin, Yongkai Li, Guan-Yong Wang, Hai-Li Huang, Sen Shao, Jinjin Liu, Peng Zhu, Nana Shumiya, Md Shafayat Hossain, Hongxiong Liu, Youguo Shi, Junxi Duan, Xiang Li, Guoqing Chang, Pengcheng Dai, Zijin Ye, Gang Xu, Yanchao Wang, Hao Zheng, Jinfeng Jia, M. Zahid Hasan, and Yugui Yao. Electronic nature of chiral charge order in the kagome superconductor CsV_3Sb_5 . *Phys. Rev. B*, 104:075148, Aug 2021. doi:10.1103/PhysRevB.104.075148. URL <https://link.aps.org/doi/10.1103/PhysRevB.104.075148>.
- [35] Ying Xiang, Qing Li, Yongkai Li, Wei Xie, Huan Yang, Zhiwei Wang, Yugui Yao, and Hai-Hu Wen. Twofold symmetry of c -axis resistivity in topological kagome superconductor CsV_3Sb_5 with in-plane rotating magnetic field. *Nat. Commun.*, 12(1):6727, 2021.
- [36] Dirk Wulferding, Seungyeol Lee, Youngsu Choi, Qiangwei Yin, Zhijun Tu, Chunsheng Gong, Hechang Lei, Saqlain Yousuf, Jaegu Song, Hanoh Lee, Tuson Park, and Kwang-Yong Choi. Emergent nematicity and intrinsic versus extrinsic electronic scattering processes in the kagome metal CsV_3Sb_5 . *Phys. Rev. Res.*, 4:023215, Jun 2022.
- [37] Qiong Wu, Z. X. Wang, Q. M. Liu, R. S. Li, S. X. Xu, Q. W. Yin, C. S. Gong, Z. J. Tu, H. C. Lei, T. Dong, and N. L. Wang. Simultaneous formation of two-fold rotation symmetry with charge order in the kagome superconductor CsV_3Sb_5 by optical polarization rotation measurement. *Phys. Rev. B*, 106:205109, Nov 2022.
- [38] Takamori Park, Mengxing Ye, and Leon Balents. Electronic instabilities of kagome metals: Saddle points and landau theory. *Phys. Rev. B*, 104:035142, Jul 2021. doi:10.1103/PhysRevB.104.035142. URL <https://link.aps.org/doi/10.1103/PhysRevB.104.035142>.
- [39] Hengxin Tan, Yizhou Liu, Ziqiang Wang, and Binghai Yan. Charge density waves and electronic properties of superconducting kagome metals. *Phys. Rev. Lett.*, 127:046401, Jul 2021. doi:10.1103/PhysRevLett.127.046401. URL <https://link.aps.org/doi/10.1103/PhysRevLett.127.046401>.
- [40] J. W. F. Venderbos. Symmetry analysis of translational symmetry broken density waves: Application to hexagonal lattices in two dimensions. *Phys. Rev. B*, 93:115107, Mar 2016. doi:10.1103/PhysRevB.93.115107. URL <https://link.aps.org/doi/10.1103/PhysRevB.93.115107>.
- [41] Note1. Note that the full three-dimensional point group is $D_{6h} = C_{6v} \otimes \sigma_h$ with σ_h denoting the mirror $z \mapsto -z$, but we restrict our considerations to C_{6v} for simplicity.
- [42] Xianxin Wu, Tilman Schwemmer, Tobias Müller, Armando Consiglio, Giorgio Sangiovanni, Domenico Di Sante, Yasir Iqbal, Werner Hanke, Andreas P. Schnyder, M. Michael Denner, Mark H. Fischer, Titus Neupert, and Ronny Thomale. Nature of unconventional pairing in the kagome superconductors AV_3Sb_5 ($A = \text{K, Rb, Cs}$). *Phys. Rev. Lett.*, 127:177001, Oct 2021. doi:10.1103/PhysRevLett.127.177001. URL <https://link.aps.org/doi/10.1103/PhysRevLett.127.177001>.
- [43] Brenden R. Ortiz, Paul M. Sarte, Eric M. Kenney, Michael J. Graf, Samuel M. L. Teicher, Ram Seshadri, and Stephen D. Wilson. Superconductivity in the Z_2 kagome metal KV_3Sb_5 . *Phys. Rev. Mater.*, 5:034801, Mar 2021. doi:10.1103/PhysRevMaterials.5.034801. URL <https://link.aps.org/doi/10.1103/PhysRevMaterials.5.034801>.
- [44] Zuwei Liang, Xingyuan Hou, Fan Zhang, Wanru Ma, Ping Wu, Zongyuan Zhang, Fanghang Yu, J.-J. Ying, Kun Jiang, Lei Shan, Zhenyu Wang, and X.-H. Chen. Three-dimensional charge density wave and surface-dependent vortex-core states in a kagome superconductor CsV_3Sb_5 . *Phys. Rev. X*, 11:031026, Aug 2021. doi:10.1103/PhysRevX.11.031026. URL <https://link.aps.org/doi/10.1103/PhysRevX.11.031026>.
- [45] Xilin Feng, Yi Zhang, Kun Jiang, and Jiangping Hu. Low-energy effective theory and symmetry classification of flux phases on the kagome lattice. *Phys. Rev. B*, 104:165136, Oct 2021. doi:10.1103/PhysRevB.104.165136. URL <https://link.aps.org/doi/10.1103/PhysRevB.104.165136>.
- [46] Morten H. Christensen, Turan Birol, Brian M. Andersen, and Rafael M. Fernandes. Loop currents in AV_3Sb_5 kagome metals: Multipolar and toroidal magnetic orders. *Phys. Rev. B*, 106:144504, Oct 2022. doi:10.1103/PhysRevB.106.144504. URL <https://link.aps.org/doi/10.1103/PhysRevB.106.144504>.
- [47] Note2. An exception would be specific gauges for flux orders with exactly 0 or π flux per plaquette. However, here we are interested in phases with generic values of flux.
- [48] Hyeok-Jun Yang, Hee Seung Kim, Min Yong Jeong, Yong Baek Kim, Myung Joon Han, and SungBin Lee. Intertwining orbital current order and superconductivity in kagome metal. *SciPost Phys. Core*, 6:008, 2023.

- doi:10.21468/SciPostPhysCore.6.1.008. URL <https://scipost.org/10.21468/SciPostPhysCore.6.1.008>.
- [49] M. Michael Denner, Ronny Thomale, and Titus Neupert. Analysis of charge order in the kagome metal AV_3Sb_5 ($A = K, Rb, Cs$). *Phys. Rev. Lett.*, 127:217601, Nov 2021. doi:10.1103/PhysRevLett.127.217601. URL <https://link.aps.org/doi/10.1103/PhysRevLett.127.217601>.
- [50] Francesco Grandi, Armando Consiglio, Michael A. Sentef, Ronny Thomale, and Dante M. Kennes. Theory of nematic charge orders in kagome metals, 2023. URL <https://arxiv.org/abs/2302.01615>.
- [51] Yu-Ping Lin and Rahul M. Nandkishore. Complex charge density waves at van hove singularity on hexagonal lattices: Haldane-model phase diagram and potential realization in the kagome metals AV_3Sb_5 ($A=K, Rb, Cs$). *Phys. Rev. B*, 104:045122, Jul 2021. doi:10.1103/PhysRevB.104.045122. URL <https://link.aps.org/doi/10.1103/PhysRevB.104.045122>.
- [52] Rina Tazai, Youichi Yamakawa, and Hiroshi Kontani. Charge-loop current order and Z3 nematicity mediated by bond-order fluctuations in kagome metal AV_3Sb_5 ($A=Cs,Rb,K$), 2022.
- [53] J. Choi, Q. Wang, S. Jöhr, N. B. Christensen, J. Küspert, D. Bucher, D. Biscette, M. H. Fischer, M. Hücker, T. Kurosawa, N. Momono, M. Oda, O. Ivashko, M. v. Zimmermann, M. Janoschek, and J. Chang. Unveiling unequivocal charge stripe order in a prototypical cuprate superconductor. *Phys. Rev. Lett.*, 128:207002, May 2022.
- [54] Vadim Grinenko, Shreenanda Ghosh, Rajib Sarkar, Jean-Christophe Orain, Artem Nikitin, Matthias Elender, Debarchan Das, Zurab Guguchia, Felix Brückner, Mark E. Barber, Joonbum Park, Naoki Kikugawa, Dmitry A. Sokolov, Jake S. Bobowski, Takuto Miyoshi, Yoshiteru Maeno, Andrew P. Mackenzie, Hubertus Luetkens, Clifford W. Hicks, and Hans-Henning Klauss. Split superconducting and time-reversal symmetry-breaking transitions in $sr2ruo4$ under stress. *Nature Physics*, 17(6):748–754, 2021.
- [55] Kevin P. Nuckolls, Ryan L. Lee, Myungchul Oh, Dillon Wong, Tomohiro Soejima, Jung Pyo Hong, Dumitru Călugăru, Jonah Herzog-Arbeitman, B. Andrei Bernevig, Kenji Watanabe, Takashi Taniguchi, Nicolas Regnault, Michael P. Zaletel, and Ali Yazdani. Quantum textures of the many-body wavefunctions in magic-angle graphene, 2023.
- [56] Rina Tazai, Youichi Yamakawa, and Hiroshi Kontani. Drastic magnetic-field-induced chiral current order and emergent current-bond-field interplay in kagome metal AV_3Sb_5 ($A=Cs,Rb,K$), 2023. URL <https://arxiv.org/abs/2303.00623>.
- [57] J. Luo, Z. Zhao, Y. Z. Zhou, J. Yang, A. F. Fang, H. T. Yang, H. J. Gao, R. Zhou, and Guo-qing Zheng. Possible star-of-david pattern charge density wave with additional modulation in the kagome superconductor CsV_3Sb_5 . *npj Quantum Materials*, 7(1):30, 2022. doi:10.1038/s41535-022-00437-7. URL <https://doi.org/10.1038/s41535-022-00437-7>.
- [58] Z. Guguchia, C. Mielke, D. Das, R. Gupta, J. X. Yin, H. Liu, Q. Yin, M. H. Christensen, Z. Tu, C. Gong, N. Shumiya, Md Shafayat Hossain, Ts. Gamsakhurdashvili, M. Elender, Pengcheng Dai, A. Amato, Y. Shi, H. C. Lei, R. M. Fernandes, M. Z. Hasan, H. Luetkens, and R. Khasanov. Tunable unconventional kagome superconductivity in charge ordered RbV_3Sb_5 and KV_3Sb_5 . *Nature Communications*, 14(1):153, 2023. doi:10.1038/s41467-022-35718-z. URL <https://doi.org/10.1038/s41467-022-35718-z>.
- [59] Rustem Khasanov, Debarchan Das, Ritu Gupta, Charles Mielke, Matthias Elender, Qiangwei Yin, Zhijun Tu, Chunsheng Gong, Hechang Lei, Ethan T. Ritz, Rafael M. Fernandes, Turan Birol, Zurab Guguchia, and Hubertus Luetkens. Time-reversal symmetry broken by charge order in CsV_3Sb_5 . *Phys. Rev. Res.*, 4:023244, Jun 2022. doi:10.1103/PhysRevResearch.4.023244. URL <https://link.aps.org/doi/10.1103/PhysRevResearch.4.023244>.
- [60] Noah Ratcliff, Lily Hallett, Brenden R. Ortiz, Stephen D. Wilson, and John W. Harter. Coherent phonon spectroscopy and interlayer modulation of charge density wave order in the kagome metal CsV_3Sb_5 . *Phys. Rev. Mater.*, 5:L111801, Nov 2021. doi:10.1103/PhysRevMaterials.5.L111801. URL <https://link.aps.org/doi/10.1103/PhysRevMaterials.5.L111801>.
- [61] Haoxiang Li, T. T. Zhang, T. Yilmaz, Y. Y. Pai, C. E. Marvinney, A. Said, Q. W. Yin, C. S. Gong, Z. J. Tu, E. Vescovo, C. S. Nelson, R. G. Moore, S. Murakami, H. C. Lei, H. N. Lee, B. J. Lawrie, and H. Miao. Observation of unconventional charge density wave without acoustic phonon anomaly in kagome superconductors AV_3sb_5 ($A = Rb, Cs$). *Phys. Rev. X*, 11:031050, Sep 2021. doi:10.1103/PhysRevX.11.031050. URL <https://link.aps.org/doi/10.1103/PhysRevX.11.031050>.
- [62] Shangfei Wu, Brenden R. Ortiz, Hengxin Tan, Stephen D. Wilson, Binghai Yan, Turan Birol, and Girsh Blumberg. Charge density wave order in the kagome metal AV_3Sb_5 ($A = Cs, Rb, K$). *Phys. Rev. B*, 105:155106, Apr 2022. doi:10.1103/PhysRevB.105.155106. URL <https://link.aps.org/doi/10.1103/PhysRevB.105.155106>.
- [63] Hengxin Tan, Yizhou Liu, Ziqiang Wang, and Binghai Yan. Charge density waves and electronic properties of superconducting kagome metals. *Phys. Rev. Lett.*, 127:046401, Jul 2021. doi:10.1103/PhysRevLett.127.046401. URL <https://link.aps.org/doi/10.1103/PhysRevLett.127.046401>.
- [64] Ece Uykur, Brenden R. Ortiz, Stephen D. Wilson, Martin Dressel, and Alexander A. Tsirlin. Optical detection of the density-wave instability in the kagome metal KV_3Sb_5 . *npj Quantum Materials*, 7(1):16, 2022. doi:10.1038/s41535-021-00420-8. URL <https://doi.org/10.1038/s41535-021-00420-8>.
- [65] Haitao Yang, Zihao Huang, Yuhang Zhang, Zhen Zhao, Jinan Shi, Hailan Luo, Lin Zhao, Guojian Qian, Hengxin Tan, Bin Hu, Ke Zhu, Zouyouwei Lu, Hua Zhang, Jianping Sun, Jinguang Cheng, Chengmin Shen, Xiao Lin, Binghai Yan, Xingjiang Zhou, Ziqiang Wang, Stephen J. Pennycook, Hui Chen, Xiaoli Dong, Wu Zhou, and Hong-Jun Gao. Titanium doped kagome superconductor $CsV_{3-x}Ti_xSb_5$ and two distinct phases. *Science Bulletin*, 67(21):2176–2185, 2022. ISSN 2095-9273. doi:https://doi.org/10.1016/j.scib.2022.10.015. URL <https://www.sciencedirect.com/science/article/pii/S2095927322004753>.
- [66] Yongkai Li, Qing Li, Xinwei Fan, Jinjin Liu, Qi Feng, Min Liu, Chunlei Wang, Jia-Xin Yin, Junxi Duan, Xiang Li, Zhiwei Wang, Hai-Hu Wen, and Yugui Yao. Tuning the competition between superconductivity

- tivity and charge order in the kagome superconductor $\text{Cs}(\text{V}_{1-x}\text{Nb}_x)_3\text{Sb}_5$. *Phys. Rev. B*, 105:L180507, May 2022. doi:10.1103/PhysRevB.105.L180507. URL <https://link.aps.org/doi/10.1103/PhysRevB.105.L180507>.
- [67] Yigui Zhong, Jinjin Liu, Xianxin Wu, Zurab Guguchia, J.-X. Yin, Akifumi Mine, Yongkai Li, Sahand Najafzadeh, Debarchan Das, Charles Mielke, Rustem Khasanov, Hubertus Luetkens, Takeshi Suzuki, Kecheng Liu, Xinloong Han, Takeshi Kondo, Jiangping Hu, Shik Shin, Zhiwei Wang, Xun Shi, Yugui Yao, and Kozo Okazaki. Nodeless electron pairing in CsV_3Sb_5 -derived kagome superconductors. *Nature*, Apr 2023. ISSN 1476-4687. doi:10.1038/s41586-023-05907-x. URL <https://doi.org/10.1038/s41586-023-05907-x>.
- [68] Yanpeng Song, Tianping Ying, Xu Chen, Xu Han, Xianxin Wu, Andreas P. Schnyder, Yuan Huang, Jian-gang Guo, and Xiaolong Chen. Competition of superconductivity and charge density wave in selective oxidized CsV_3Sb_5 thin flakes. *Phys. Rev. Lett.*, 127:237001, Dec 2021. doi:10.1103/PhysRevLett.127.237001. URL <https://link.aps.org/doi/10.1103/PhysRevLett.127.237001>.
- [69] Boqin Song, Tianping Ying, Xianxin Wu, Wei Xia, Qiangwei Yin, Qinghua Zhang, Yanpeng Song, Xiaofan Yang, Jiangang Guo, Lin Gu, Xiaolong Chen, Jiangping Hu, Andreas P. Schnyder, Hechang Lei, Yanfeng Guo, and Shiyang Li. Anomalous enhancement of charge density wave in kagome superconductor CsV_3Sb_5 approaching the 2d limit. *Nature Communications*, 14(1):2492, 2023. doi:10.1038/s41467-023-38257-3. URL <https://doi.org/10.1038/s41467-023-38257-3>.
- [70] B. Q. Song, X. M. Kong, W. Xia, Q. W. Yin, C. P. Tu, C. C. Zhao, D. Z. Dai, K. Meng, Z. C. Tao, Z. J. Tu, C. S. Gong, H. C. Lei, Y. F. Guo, X. F. Yang, and S. Y. Li. Competing superconductivity and charge-density wave in kagome metal CsV_3Sb_5 : evidence from their evolutions with sample thickness, 2021.
- [71] B. Fauqué, Y. Sidis, V. Hinkov, S. Pailhès, C. T. Lin, X. Chaud, and P. Bourges. Magnetic order in the pseudogap phase of high- T_C superconductors. *Phys. Rev. Lett.*, 96:197001, May 2006. doi:10.1103/PhysRevLett.96.197001. URL <https://link.aps.org/doi/10.1103/PhysRevLett.96.197001>.
- [72] Sayak Ghosh, Arkady Shekhter, F. Jerzembeck, N. Kikugawa, Dmitry A. Sokolov, Manuel Brando, A. P. Mackenzie, Clifford W. Hicks, and B. J. Ramshaw. Thermodynamic evidence for a two-component superconducting order parameter in Sr_2RuO_4 . *Nature Physics*, 17(2):199–204, 2021. doi:10.1038/s41567-020-1032-4. URL <https://doi.org/10.1038/s41567-020-1032-4>.
- [73] J. C. Slonczewski and H. Thomas. Interaction of elastic strain with the structural transition of strontium titanate. *Phys. Rev. B*, 1:3599–3608, May 1970. doi:10.1103/PhysRevB.1.3599. URL <https://link.aps.org/doi/10.1103/PhysRevB.1.3599>.
- [74] R G Leisure and F A Willis. Resonant ultrasound spectroscopy. *Journal of Physics: Condensed Matter*, 9(28):6001, jul 1997. doi:10.1088/0953-8984/9/28/002. URL <https://dx.doi.org/10.1088/0953-8984/9/28/002>.

— Supplementary Material —
Phenomenology of bond and flux orders in kagome metals

Glenn Wagner, Chunyu Guo, Philip J. W. Moll, Titus Neupert, Mark H. Fischer

Appendix A: Group theory details

	I	t_i	C_2	$t_i C_2$	C_3	C_6	σ_v	$t_i \sigma_v$	σ_d	$t_i \sigma_d$
$ C $	1	3	1	3	8	8	6	6	6	6
A_1	1	1	1	1	1	1	1	1	1	1
A_2	1	1	1	1	1	1	-1	-1	-1	-1
B_1	1	1	-1	-1	1	-1	1	1	-1	-1
B_2	1	1	-1	-1	1	-1	-1	-1	1	1
E_1	2	2	-2	-2	-1	1	0	0	0	0
E_2	2	2	2	2	-1	-1	0	0	0	0
F_1	3	-1	3	-1	0	0	1	-1	1	-1
F_2	3	-1	3	-1	0	0	-1	1	-1	1
F_3	3	-1	-3	1	0	0	1	-1	-1	1
F_4	3	-1	-3	1	0	0	-1	1	1	-1

TABLE I. Character table of the group C_{6v}''' .

For the site order, we compute the permutation matrix $\mathcal{P}_s(g)$ that describes how the sites transform into each other under the operation $g \in C_{6v}'''$. Since there are 12 sites in the 2×2 enlarged unit cell, the set of permutation matrices describe a 12-dimensional reducible representation of C_{6v}''' . In order to decompose this representation into irreps, we compute the characters $\chi(g) = \text{Tr}(\mathcal{P}_s(g))$, in other words, we count the number of sites that map to themselves under the operations of C_{6v}''' . We find

g	I	t_i	C_2	$t_i C_2$	C_3	C_6	σ_v	$t_i \sigma_v$	σ_d	$t_i \sigma_d$
$\frac{g}{\text{Tr}(\mathcal{P}_s(g))}$	12	0	0	4	0	0	2	0	2	0

We can then compute the multiplicity n_R of the irrep R in the decomposition of this reducible representation via

$$n_R = \frac{1}{|C_{6v}'''} \sum_{g \in C_{6v}'''} \chi_R(g) \chi(g), \quad (\text{A1})$$

where the characters $\chi_R(g)$ are listed in the character table (Tab. I). This leads to the decomposition of site order

$$\mathcal{P}_s = A_1 + E_2 + F_1 + F_3 + F_4. \quad (\text{A2})$$

The bond and flux order can be treated similarly.

Appendix B: Multiplication table of irreps of C_{6v}'''

We want to decompose the product of two irreps R_i and R_j into a sum of irreps

$$R_i \otimes R_j = \bigoplus_k n_k R_k, \quad (\text{B1})$$

where

$$n_k = \frac{1}{|C_{6v}'''} \sum_{g \in C_{6v}'''} \chi_k(g) \chi_i(g) \chi_j(g). \quad (\text{B2})$$

We list the results in Tab. II.

Appendix C: Coupling to strain

The crucial symmetry to determine the coupling to strain is C_3 . The components of the strain tensor transform in the E irrep, which transforms non-trivially under C_3 , and so in order to obtain a scalar (i.e. a term that we can add to the free energy), we need to construct a term out of the order parameter that also transforms under the E irrep. The basis functions of the E irrep are conventionally labelled as $p_{\pm} = p_x \pm ip_y$ which pick up phases of $\omega = e^{2\pi i/3}$ and ω^* respectively under C_3 . Looking at the transformation properties of the order parameter under C_3 , we find that the quadratic terms that transform correctly are

$$p_+ = \Delta_1^2 + \omega\Delta_2^2 + \omega^2\Delta_3^2, \quad (C1)$$

$$p_- = \Delta_1^2 + \omega^2\Delta_2^2 + \omega\Delta_3^2, \quad (C2)$$

where $\omega = e^{2\pi i/3}$. Then we write these as $p_{\pm} = (p_x \pm ip_y)$ with

$$p_x = \Delta_1^2 - \Delta_2^2/2 - \Delta_3^2/2, \quad (C3)$$

$$p_y = \frac{\sqrt{3}}{2}(\Delta_2^2 - \Delta_3^2). \quad (C4)$$

One can check that the doublet $\{p_x, p_y\}$ transforms in the same way under C_3 as $\{\epsilon_{p_x}, \epsilon_{p_y}\} = \{(\epsilon_{xx} - \epsilon_{yy})/2, \epsilon_{xy}\}$, allowing us to construct the C_3 -symmetric term to be added to the free energy:

$$\mathcal{F}^{(\text{str})} = 2\mu_2(\epsilon_{p_x}p_x + \epsilon_{p_y}p_y) = \mu_2[(\epsilon_{xx} - \epsilon_{yy})(\Delta_1^2 - \Delta_2^2/2 - \Delta_3^2/2) + \epsilon_{xy}\sqrt{3}(\Delta_2^2 - \Delta_3^2)]. \quad (C5)$$

The analogous term for flux order automatically respects time-reversal symmetry since it is quadratic in the order parameter and hence flux order couples to strain in the same manner (with a different coupling coefficient).

The coupling to strain gives us a way to quantify the anisotropy in the system. For an isotropic phase, the order parameters p_x and p_y will be zero. If the solution is anisotropic, there will be degenerate solutions with different values of p_x and p_y and application of strain will pick out one of these degenerate solutions leading to divergent susceptibility. Let us consider the response to strain in the system at finite temperature T . The expectation value of the symmetry-breaking order parameter is

$$\langle p_x \rangle_{\mathcal{F}(\epsilon_{p_x}), T} = \langle p_x e^{-\beta\mathcal{F}^{(\text{str})}} \rangle_{0, T} = \langle p_x e^{-2\beta\mu_2\epsilon_{p_x}p_x} \rangle_{0, T}, \quad (C6)$$

where $\langle \dots \rangle_{0, T}$ denotes the finite-temperature average with respect to the zero-strain free energy $\mathcal{F}(\epsilon_{p_x} = 0)$ and $\beta = 1/(k_B T)$. The susceptibility is then

$$\chi_{p_x} = \lim_{\epsilon_{p_x} \rightarrow 0} \frac{\partial \langle p_x \rangle_{\mathcal{F}(\epsilon_{p_x}), T}}{\partial \epsilon_{p_x}} = -2\beta\mu_2 \langle p_x^2 \rangle_{0, T}, \quad (C7)$$

and similarly $\chi_{p_y} = -2\beta\mu_2 \langle p_y^2 \rangle_{0, T}$. The susceptibilities diverge when $T \rightarrow 0$ if p_x^2 or p_y^2 acquire a finite expectation value in the ground state. This is the signature of spontaneous symmetry breaking. This motivates us to introduce the anisotropic order parameter

$$\frac{1}{\beta} \text{Tr}\chi = \frac{1}{\beta} (\chi_{p_x} + \chi_{p_y}) = -2\mu_2(p_x^2 + p_y^2) = -4\beta\mu_2 \sum_{i,j} (\Delta_i^2 - \Delta_j^2)^2 \quad (C8)$$

and an analogous order parameter can be written down for the flux order.

Appendix D: First-order transition

When $T_c \sim T'_c$, there is a first-order transition into a phase with both charge and flux order. Let us consider the free energy

$$\mathcal{F} = \alpha(T - T_c)\Delta^2 + \alpha(T - T'_c)\Delta'^2 + b\Delta\Delta'^2 + c(\Delta^2 + \Delta'^2)^2 = A\psi^2 + B\psi^3 + C\psi^4 \quad (D1)$$

where we used the parametrization $\Delta + i\Delta' = \psi e^{i\phi}$ and

$$A = \alpha(T - T_c) \cos^2 \phi + \alpha(T - T'_c) \sin^2 \phi = \alpha[T - T_c \cos^2 \phi - T'_c \sin^2 \phi] \quad (D2)$$

$$B = b \cos \phi \sin^2 \phi \quad (D3)$$

$$C = c. \quad (D4)$$

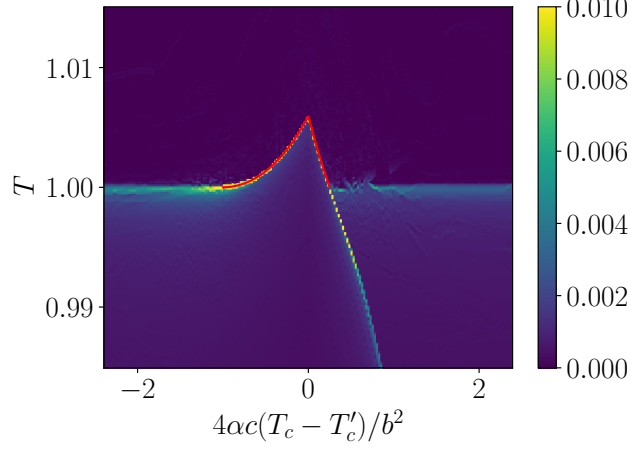
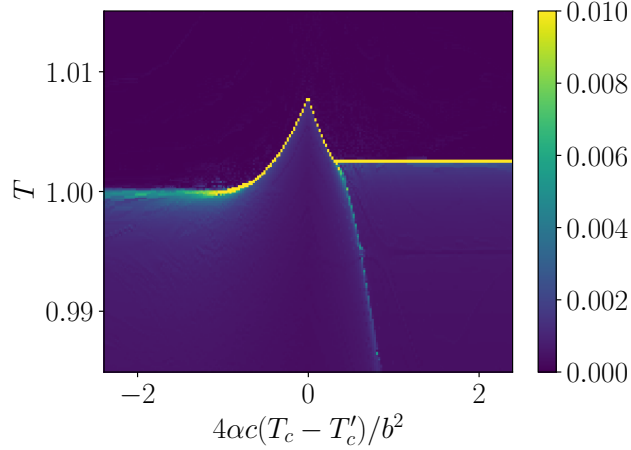
(a) case with $d = 0$ (b) case with $d = b/4$

FIG. S1. Temperature derivative of the order parameter amplitude $\Delta^2 + \Delta'^2$ for the free energy (D1) with a term $d\Delta^3$. Large values of the derivative (yellow) indicate first order phase transitions. (a) In the case $d = 0$, there is a first order transition for a finite range of $T_c - T'_c$. The red curves show the analytical results (D6) and (D8). (b) In the case $d > 0$, there is a first order phase transition for all $T_c > T'_c$.

The minimum of the free energy is at a non-zero value of the order parameter when $A < \frac{B^2}{4C}$ i.e. when

$$T < T_1 = T_c \cos^2 \phi + T'_c \sin^2 \phi + \frac{b^2}{4\alpha c} \cos^2 \phi \sin^4 \phi = T_c + (T'_c - T_c)[\sin^2 \phi + \eta(\sin^4 \phi - \sin^6 \phi)], \quad (\text{D5})$$

where $\eta = b^2/[4\alpha c(T'_c - T_c)]$. We will have a first-order transition, when there is a non-zero solution at $T > T_c, T'_c$. Consider first the case where $T'_c > T_c$. Maximizing the term in square brackets leads to

$$\max_{\phi}(T_1) = T_c + (T'_c - T_c) \frac{(\eta + \sqrt{\eta(3 + \eta)})(6 + \eta + \sqrt{\eta(3 + \eta)})}{27\eta}, \quad (\text{D6})$$

when $\sin^2 \phi = (\eta + \sqrt{\eta(3 + \eta)})/(3\eta) \leq 1$. We have $\max_{\phi}(T_1) > T'_c$ when $\eta > 1$. Similarly, when $T_c > T'_c$, we can write

$$T_1 = T'_c + (T_c - T'_c)[\cos^2 \phi - \eta \cos^2 \phi(1 - \cos^2 \phi)^2]. \quad (\text{D7})$$

Maximizing with respect to ϕ yields

$$\max_{\phi}(T_1) = T'_c + (T_c - T'_c) \frac{2(2\eta + \sqrt{\eta(3+\eta)})(3 - \eta + \sqrt{\eta(3+\eta)})}{27\eta}, \quad (\text{D8})$$

and $\max_{\phi}(T_1) > T_c$ when $\eta < -4$. So we have a first-order transition in a range where the critical temperatures of the two orders are similar:

$$\frac{b^2}{4\alpha c} > (T'_c - T_c) > -\frac{b^2}{16\alpha c}. \quad (\text{D9})$$

Appendix E: Anisotropy from third-order term

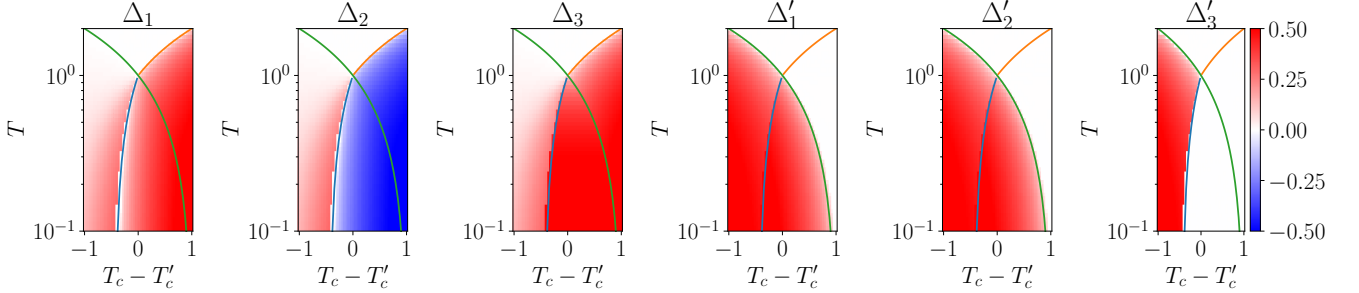


FIG. S2. We plot the six order parameters and the phase boundaries between the different solutions. The blue line shows the boundary between solution 1 and solution 2 ($\sim T^*$), while the green line shows the boundary between solution 3 and solution 4 ($\sim T'_c$). In between the blue and green lines there is a crossover from solution 2 to solution 3. The yellow lines shows the onset of Δ order ($\sim T_c$). The wedge between the blue and green lines is where the solution is anisotropic.

Anisotropy can arise from the third-order term in the free energy even when the fourth-order terms favor an isotropic solution. To see this, consider the terms

$$\mathcal{F}^{(3)} = \beta_1 \Delta_1 \Delta_2 \Delta_3 + \beta_2 (\Delta_1 \Delta'_2 \Delta'_3 + \Delta'_1 \Delta_2 \Delta'_3 + \Delta'_1 \Delta'_2 \Delta_3) \quad (\text{E1})$$

as perturbations with $\Delta^2 = \Delta_1^2 + \Delta_2^2 + \Delta_3^2$ and $\Delta'^2 = \Delta'^2_1 + \Delta'^2_2 + \Delta'^2_3$ being fixed by the second-order and fourth-order terms in the free energy. The results derived below will therefore be exact in the limit $\beta_1 \rightarrow 0$, $\beta_2 \rightarrow 0$, though the numerics demonstrate that the results are similar for finite β_1, β_2 . We study the case $\beta_1 \beta_2 < 0$. The signs of β_1 and β_2 can always be flipped by changing the sign of Δ_i , so without loss of generality, we assume $\beta_1 > 0$ and $\beta_2 < 0$. We now study the competition between four different solutions of the free energy, which will be the ground states as we traverse the phase diagram in Fig. S2 from left to right.

- Solution 1: $\Delta_1 = \Delta_2 = \Delta_3 = \frac{\Delta}{\sqrt{3}}$ and $\Delta'_1 = \Delta'_2 = \Delta'_3 = \frac{\Delta'}{\sqrt{3}}$ leads to $\mathcal{F}^{(3)} = \frac{|\beta_1|}{3\sqrt{3}} \Delta^3 - \frac{|\beta_2|}{\sqrt{3}} \Delta \Delta'^2$
- Solution 2: $\Delta_3 = \Delta$ and $\Delta'_1 = \Delta'_2 = \frac{\Delta'}{\sqrt{2}}$ leads to $\mathcal{F}^{(3)} = -\frac{|\beta_2|}{2} \Delta \Delta'^2$
- Solution 3: $\Delta_1 = -\Delta_2 = \Delta_3 = \frac{\Delta}{\sqrt{3}}$ and $\Delta'_1 = \Delta'_2 = \frac{\Delta'}{\sqrt{2}}$ leads to $\mathcal{F}^{(3)} = -\frac{|\beta_1|}{3\sqrt{3}} \Delta^3 - \frac{|\beta_2|}{2\sqrt{3}} \Delta \Delta'^2$
- Solution 4: $\Delta_1 = -\Delta_2 = \Delta_3 = \frac{\Delta}{\sqrt{3}}$ and $\Delta'_i = 0$ leads to $\mathcal{F}^{(3)} = -\frac{|\beta_1|}{3\sqrt{3}} \Delta^3$

Let us further assume second-order terms $\mathcal{F}^{(2)} = \alpha(T - T_c)\Delta^2 + \alpha(T - T'_c)\Delta'^2$ and fourth-order terms $\mathcal{F}^{(4)} = \lambda(\Delta^4 + \Delta'^4)$ such that

$$\Delta^2 = \frac{\alpha(T_c - T)}{2\lambda}, \quad (\text{E2})$$

$$\Delta'^2 = \frac{\alpha(T'_c - T)}{2\lambda}. \quad (\text{E3})$$

Comparing the energies of solution 1 and solution 2, we find that the transition occurs at

$$T^* = \frac{T_c - \zeta T'_c}{1 - \zeta}, \quad (\text{E4})$$

where $\zeta = 3(1 - \frac{\sqrt{3}}{2})|\beta_2|/|\beta_1|$. We plot this transition temperature as a blue line in Fig. S2. Solutions 1 and 4 are isotropic, while solutions 2 and 3 are anisotropic.

Appendix F: Anisotropy in the presence of a magnetic field

The magnetic field adds a term to the free energy

$$\mathcal{F}^{(B)} = \mu_1 B (\Delta_1 \Delta'_1 + \Delta_2 \Delta'_2 + \Delta_3 \Delta'_3). \quad (\text{F1})$$

The effect of the magnetic field is to induce Δ' as soon as Δ is present. Let us assume without loss of generality $B < 0$ (we can always switch the sign of Δ'_i to adapt to the sign of B). Of the four solutions, the only solution that can take advantage of $\mathcal{F}^{(B)}$ and lower its energy is solution 1, which has a contribution $-B\Delta\Delta'$. None of the other solutions have changes in energy to this order in the perturbation theory. Therefore solution 1 becomes more stable and the boundary between solution 1 and solution 2 shifts to the right, this is shown in Fig. S3. The result of this effects is that the magnetic field can increase the anisotropy of the order parameters, as shown in Figs. S4 and S5. In particular, due to the phase boundary between solution 1 and solution 2 shifting to the right, the value of Δ is larger, when the components become anisotropic and this results in a larger anisotropy. We note that if we are in the part of the phase diagram where $T_c < T'_c$ then the magnetic field has the opposite effect and suppresses the anisotropy (Fig. S6).

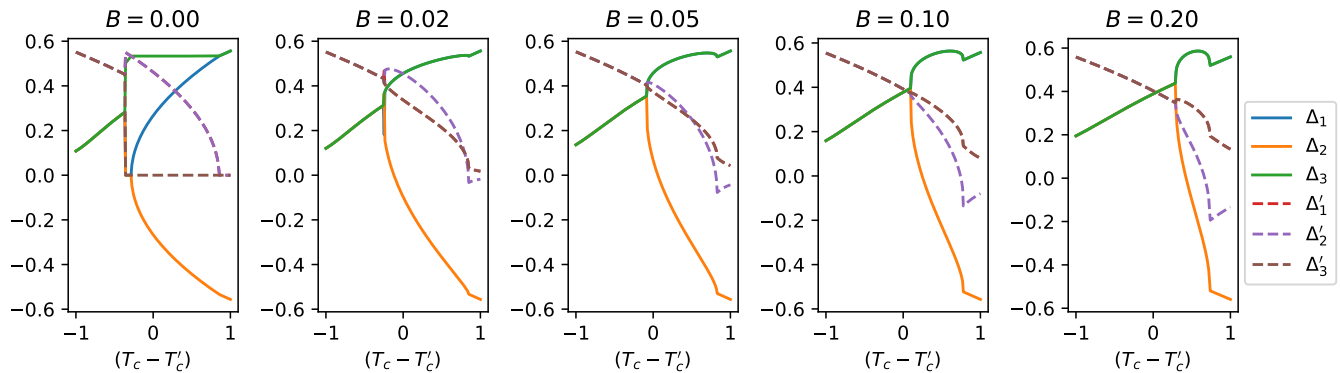


FIG. S3. We plot the six order parameters for a set of different magnetic fields. The order parameters are computed at a fixed temperature as a function of $T_c - T'_c$. For $B = 0$ we see the transitions between the four different solutions described in appendix E. The region where solution is most stable (at the left of the phase diagram) becomes larger as the B -field increases.

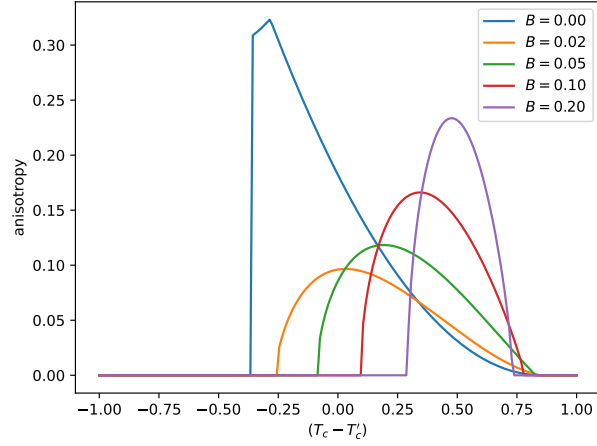


FIG. S4. We plot order parameter of the anisotropy $\sum_{i,j}[(\Delta_i^2 - \Delta_j^2)^2 + (\Delta_i'^2 - \Delta_j'^2)^2]$ for a set of different magnetic fields. We fix the temperature $T = 0.2$. We plot the anisotropy at a fixed temperature as a function of $T_c - T'_c$. There is a range of $T_c - T'_c$, where the magnetic field significantly enhances the anisotropy.

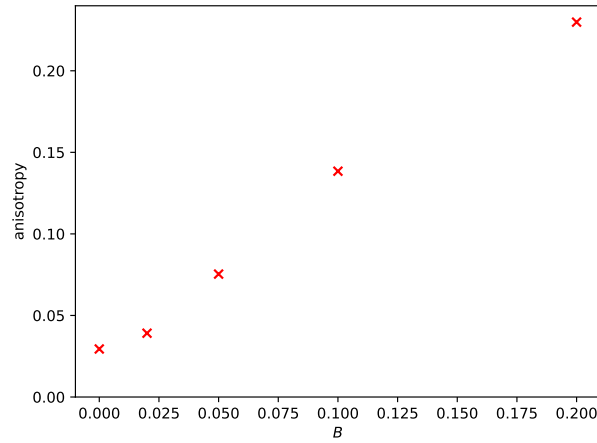


FIG. S5. Increase of the anisotropy $\sum_{i,j}[(\Delta_i^2 - \Delta_j^2)^2 + (\Delta_i'^2 - \Delta_j'^2)^2]$ as a function of the applied field. We fix $T_c - T'_c = 0.5$ and $T = 0.2$.

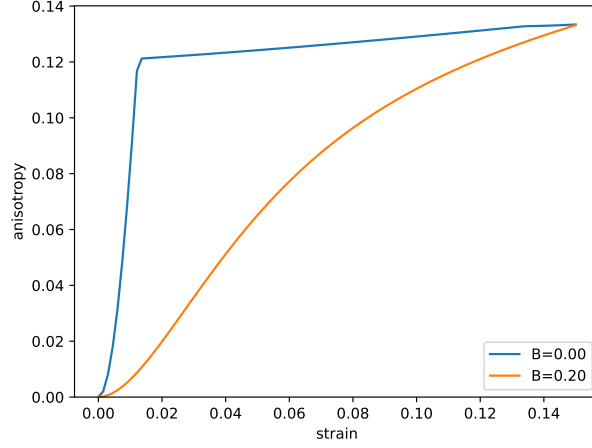
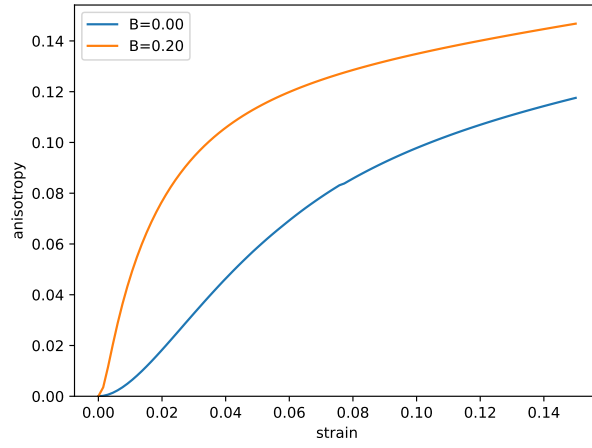
(a) case with $T_c - T'_c = -0.5$ (b) case with $T_c - T'_c = 0.5$

FIG. S6. Increase of the anisotropy $\sum_{i,j} [(\Delta_i^2 - \Delta_j^2)^2 + (\Delta_i'^2 - \Delta_j'^2)^2]$ as a function of the applied strain for two different values of the magnetic field. We fix $T = 0.55$. In the case $T_c > T'_c$ the application of the magnetic field increases the anisotropy, consistent with the experimental results from Ref. [24].